ADVANCES IN ATOMIC AND MOLECULAR PHYSICS, VOL. 22

DOUBLY EXCITED STATES, INCLUDING NEW CLASSIFICATION SCHEMES

C. D. LIN

Department of Physics
Kansas State University
Manhattan, Kansas 66506

I. Introduction

Since the birth of nonrelativistic quantum mechanics, the independent particle approximation has served as the backbone of almost all areas of microscopic physics. In atomic physics, the independent electron approximation assumes that, to first order, an atom is made of a collection of independent electrons, and the motion of each electron is determined by an averaged potential due to the nucleus and the other electrons. This approximation, whether it is in the form of the Hartree–Fock model or its equivalents, has been used to explain qualitatively as well as semiquantitatively a wealth of experimental observations. Over the last half-century, a major part of the effort in theoretical atomic physics has been devoted to finding different ways of accounting for the deviations of experimental results from the predictions of the independent electron approximation. Different methods, such as many-body perturbation theory, the configuration-interaction (CI) method, and many other perturbative approaches, have been shown to be capable of accounting for these deviations accurately. When the deviation from the prediction of the independent electron approximation is large, as happens in several isolated spectral lines, the situation can often be attributed to localized "interactions" between a few states. Such situations are amenable to the treatment of the configuration interaction method.

Since the early observation of the absorption spectra of doubly excited states of He by Madden and Codling (1963, 1965) using synchrotron radiation, it was recognized immediately by Fano and coworkers that a complete understanding of these new states requires a fundamental departure from the conventional independent particle approach. Not only should the spectral observation be explained, but a desirable new approach should also provide

the framework whereby all doubly excited states of atoms and molecules could be studied. In other words, a new approach should supply the proper language such as new quantum numbers, new systematics of spectral behavior, approximate selection rules, etc., which are also applicable to doubly excited states of other atoms. Thus one of the goals in the interpretation of doubly excited states of He is to provide this language, analogous to the study of hydrogen atoms to provide a proper language for the independent particle approximation.

The early photoabsorption spectra of doubly excited states of He indicated that among the three possible $^1P^0$ Rydberg series that converge to the $N = 2$ limit of He^+, only one series is prominently observed, while a second series is weakly visible and a third series is completely absent (Madden and Codling, 1963, 1965). In a later experiment, Woodruff and Samson (1982) measured the photoelectron spectra at higher photon energies. Their results for doubly excited states of He below the $N = 3$, 4, and 5 limits of He^+ are reproduced here in Fig. 1. According to the conventional selection rules for photoabsorption, there are 5, 7, and 9 possible Rydberg series, respectively, of doubly excited states converging to each of the limits. There was, however, only one prominent series observed in each case. Similarly, in the photodetachment of H^- for $^1P^0$ doubly excited states below the $H(N = 6)$ limit, all the resonances observed belong to the same series (H. C. Bryant, 1981; private communication). A desirable theoretical approach should provide not only a method of calculating the position and width of each doubly excited state but also the approximate selection rules for different excitation processes.

There are many theoretical approaches which are capable of predicting an accurate position and width of each doubly excited state. These methods, such as the configuration interaction method, the Feshbach projection technique, the close-coupling method, and the complex coordinate rotation technique and others, provided a wealth of "numerical" data which are essential to sorting out the systematics of doubly excited states. The contribution from these calculations cannot be underestimated. This is particularly true for doubly excited states since experimental data are so scarce. Even if these data do exist, the resolution is not good enough to extract their systematics. Furthermore, it seems clear now that some doubly excited states are not easily populated in some experiments.

The main limitation of the above-mentioned approaches is that each doubly excited state is calculated separately while experimental data indicate that the selection rule is a property of a series (or a channel). Furthermore, the results from these types of calculations are sometimes unexpected or difficult to explain. As an example, one can predict the approximate positions of doubly excited states by performing a limited CI calculation. In Table I, the results of such a calculation for the $^1P^0$ doubly excited states

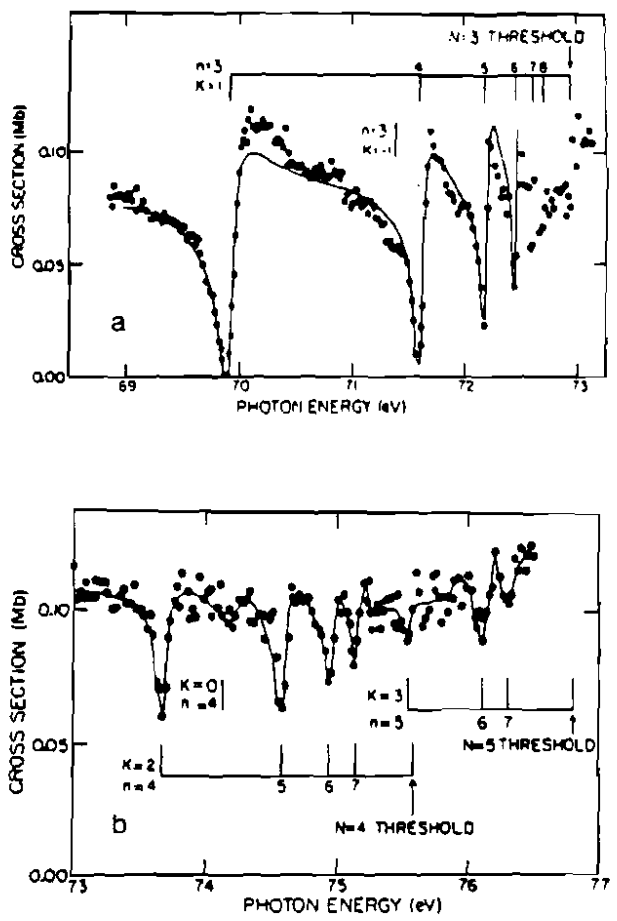

FIG. 1. The cross section for the autoionizing region of He doubly excited states below the $N = 3$, 4, and 5 thresholds of He^+. The quantum number K and the principal quantum number n of the series are indicated (Woodruff and Samson, 1982).

TABLE I

CI COEFFICIENTS OF THE FIRST THREE LOWEST DOUBLY EXCITED STATES OF He ^1P BELOW THE $He^+(N = 3)$ THRESHOLD

State	Energy (Ry)	$3s3p$	$3p3d$	$3s4p$	$3p4s$	$3p4d$	$3d4p$	$3d4f$
1	−0.667	0.683	0.616	−0.127	−0.172	−0.239	−0.203	−0.104
2	−0.563	−0.003	−0.005	0.630	−0.630	0.330	−0.304	0.068
3	−0.554	0.503	−0.557	−0.226	−0.317	−0.054	0.231	0.476

below $He^+(N = 3)$ are shown. According to conventional wisdom, one would expect that the wave function of the two lowest states are the linear combination of $3s3p$ and $3p3d$. The calculation shows that this is indeed the case for the lowest state. The second-lowest state, however, is actually mostly a linear combination of $3s4p$, $3p4s$, $3p4d$, $3d4p$, ... etc. It is the third-lowest state which is again predominantly a mixture of $3s3p$ and $3p3d$. This example serves to illustrate the limitation of the conventional approaches. When the admixture of many configurations is substantial for a given state, the meaning of configuration for that state is lost. Information about electron correlations in these approaches is embedded awkwardly in the mixing coefficients. These coefficients provide no direct clues as to how the electrons are correlated.

One of the goals of studying doubly excited states is to find a new way of characterizing electron correlations. More precisely, we want to find a new set of quantum numbers which characterize the correlations between two excited electrons. We also want to know the physical or geometrical interpretation of these quantum numbers and possible new spectroscopic regularities. In this article, our objective is to present the progress toward this goal up to this time.

The study of doubly excited states described in this article is based mostly upon the geometrical interpretation of the motion of two excited electrons. Our major task is to unravel how electrons are correlated by examining the wave functions in hyperspherical coordinates. This coordinate system is particularly suitable for analyzing electron correlations. By assuming that the mass of the nucleus is infinite, the configuration of the two electrons is described by six coordinates. Three of these coordinates are used to describe the rotation of the whole atom. In hyperspherical coordinates, among the three remaining we use one coordinate to describe the size of the atom and the two others to describe the relative orientations of the two electrons. The correlation quantum numbers are related to the nodal structure in these two angles.

The rest of this article is organized as follows. In Section II, we discuss the qualitative aspects of radial and angular correlations. The correlation quantum numbers and the classification scheme are presented in Section III. This section also contains the illustration of isomorphic correlations of states which have identical correlation quantum numbers and the existence of a supermultiplet structure. After a short digression on computational methods in Section IV, the correlation quantum numbers are re-examined by analyzing the wave functions in the body frame of the atom in Section V. The existence of approximate moleculelike normal modes of doubly excited states and its limited interpretation are also discussed in Section V. In Section VI, the effects of strong electric fields on the resonances of H^- are discussed. Doubly excited states of multielectron atoms are briefly discussed in Section VII. Several final remarks and future perspectives are given in Section VIII.

There are other studies aimed at the understanding of the systematics of doubly excited states. These include the group-theoretical approach (Wulfman, 1973; Crane and Armstrong, 1982; Herrick, 1983, and references therein), the algebraic approach (Iachello and Rau, 1981), and the analysis of the electron correlation of model two-electron systems (Ezra and Berry, 1982, 1983). The group-theoretical approach also aims at the classification of doubly excited states. All of these approaches treat the correlations of individual states. In the hyperspherical approach the correlation is studied for each channel and thus any state belonging to that channel has similar correlation properties. These other approaches, particularly the group-theoretical approach, complemented the analysis of correlations in hyperspherical coordinates presented here. A review of the group-theoretical approach has been given by Herrick (1983). The applications of the complex-coordinate rotation method to doubly excited states have been reviewed recently by Ho (1983). The analysis of electron correlations from the hyperspherical coordinates viewpoint has also been reviewed by Fano (1983). References to earlier works can be found in that article. In this review, we concentrate on the progress made since then.

II. Analysis of Radial and Angular Correlations

In this section we describe the correlations of doubly excited states as revealed through the examination of wave functions in hyperspherical coordinates. After a brief outline of the basic equations and a discussion of the quasiseparable approximation where the concept of channels is defined, we examine the meaning and the nature of radial and angular correlations for some typical channels. The discussion in this section is limited mostly to $L = 0$ states. In describing correlations, we always concentrate on the correlation of a given channel rather than that of each individual state. This is possible because the correlations for states belonging to the same channel are similar. Graphical display of correlations for each individual state has been explored by Berry and coworkers (Ezra and Berry, 1982, and references therein) using a density function $\rho(r_1, \theta_{12}, r_2)$ which measures the probability of finding electron 1 at a distance r_1 from the nucleus and with interelectronic angle θ_{12} given that electron 2 is at a distance r_2 from the nucleus.

A. The Hyperspherical Coordinates

To describe the motion of two electrons in the field of a nucleus, six coordinates are needed. One can choose three coordinates, such as the three Euler angles, to describe the overall rotation of the system and the other three to describe the internal degrees of freedom. Let us start with atomic states which have $L = 0$; their wave functions do not depend on external rotational coordinates. The internal coordinates can be chosen as the distances r_1 and r_2 of the two electrons and the angle θ_{12}. It is also possible to replace r_1 and r_2 by R and α, where

$$R = (r_1^2 + r_2^2)^{1/2}; \qquad \alpha = \tan^{-1}(r_2/r_1) \tag{1}$$

(see Fig. 2). This latter set has the advantage that R specifies the "size" of the atom and does not enter into the description of electron correlations directly. Electron correlations are then described by the two angles α and θ_{12} only. We refer to the correlation depicted by the angle α as radial correlation and to the correlation described by the angle θ_{12} as angular correlation. The correlation quantum numbers for characterizing doubly excited states provide information about radial and angular correlations of the two electrons.

For $L \neq 0$ states, the overall rotation of the atom has to be considered. Instead of using the Euler angles, computationally it is more convenient to use α, $\hat{r}_1$, and $\hat{r}_2$, where $\hat{r}_i = (\theta_i, \phi_i)$ denotes the spherical angles of electron i, as the five hyperspherical angles. To describe the internal correlations for $L \neq 0$ states, the rotation of the atom will be averaged (see Section III,C).

At this point it is convenient to introduce the Schrödinger equation for two-electron atoms in hyperspherical coordinates. Denoting the five angles α, $\hat{r}_1$, $\hat{r}_2$ collectively by Ω, the Schrödinger equation for two-electron atoms, written using atomic units, is (Macek, 1968; Lin, 1974b)

$$\left(-\frac{d^2}{dR^2} + \frac{\Lambda^2 + 15/4}{R^2} + \frac{2C}{R} - 2E\right)(R^{5/2}\psi) = 0 \tag{2}$$

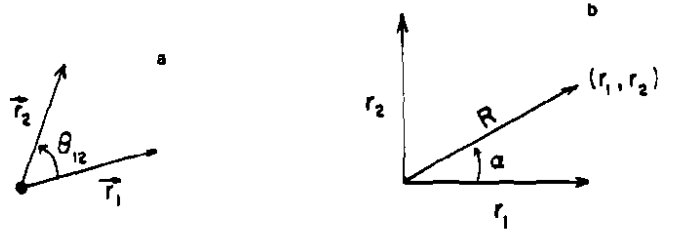

FIG. 2. (a) Diagram of the two-electron configuration. (b) Diagram to illustrate the relation between Cartesian and hyperspherical radial coordinates (Fano and Lin, 1975).

where

$$\Lambda^2 = -\frac{1}{\sin^2\alpha\cos^2\alpha}\frac{d}{d\alpha}\left(\sin^2\alpha\cos^2\alpha\frac{d}{d\alpha}\right) + \frac{l_1^2}{\cos^2\alpha} + \frac{l_2^2}{\sin^2\alpha} \tag{3}$$

is the square of the grand angular momentum operator and

$$C = -\frac{Z}{\cos\alpha} - \frac{Z}{\sin\alpha} + \frac{1}{(1 - \sin 2\alpha\cos\theta_{12})^{1/2}} \tag{4}$$

is the effective charge. This effective charge C includes both the electron–nucleus and electron–electron interactions. In Eq. (4), Z is the charge of the nucleus.

Equation (2) shows that the eigenvalue of Λ^2/R^2 acts like a centrifugal potential barrier for the simultaneous penetration of the two electrons into the small-R region. It depends not only on the orbital angular momentum of each electron, but also on the degree of radial correlation as represented by the α-dependent operator in Eq. (3). The effective charge C depends only on the relative coordinates α and θ_{12}. In Fig. 3 we display the relief map of C on the (α,θ_{12}) plane for $Z = 1$. The ordinates represent the potentials at $R = 1$. In the limit of $\alpha \to 0$ (or $\alpha \to \pi/2$), the potential surface has a sharp drop caused by the electron–nucleus attraction. This potential valley corresponds

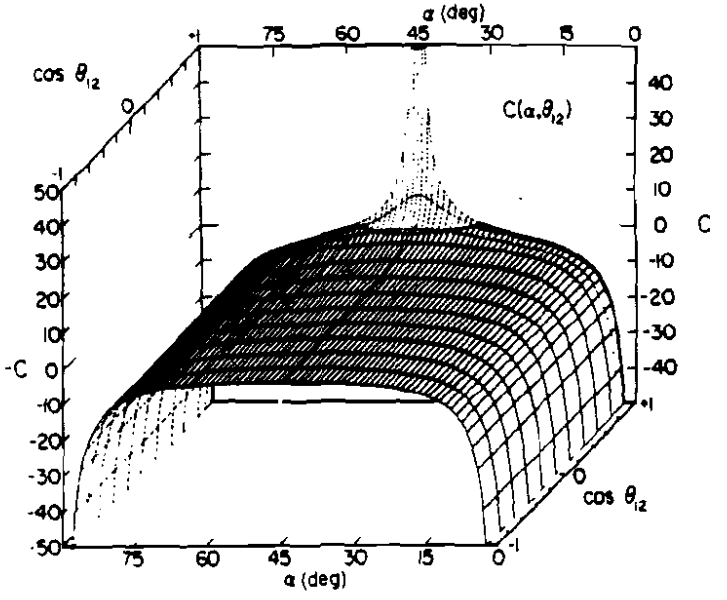

FIG. 3. Potential function $C(\alpha,\theta_{12})$ in Rydberg units for a pair of electrons in the field of a proton.

to the case in which one electron is near the nucleus and the other is far out. In the region where $r_1 = r_2$, which corresponds to $\alpha = 45°$, the potential energy depends critically on whether θ_{12} is approximately 0 or π. When $\theta_{12} = 0$ and $\alpha = 45°$, the two electrons are nearly on top of each other where the electron–electron repulsion causes the sharp spike seen in Fig. 3. We also note that $\alpha = 45°$ and $\theta_{12} = 180°$ is a saddle point; the potential is unstable away from $\alpha = 45°$, while it is stable at $\theta_{12} = 180°$ along the coordinate θ_{12}.

The Schrödinger Eq. (2) can be solved by expanding the total wave function as

$$\Psi^n_\mu(R,\Omega) = \sum_\mu F^n_\mu(R)\Phi_\mu(R;\Omega)/(R^{5/2}\sin\alpha\cos\alpha) \tag{5}$$

where μ identifies the channel and n denotes the nth state within that channel. The channel function $\Phi_\mu(R;\Omega)$ satisfies the differential equation

$$\frac{1}{R^2}\left(-\frac{d^2}{d\alpha^2} + \frac{l_1^2}{\cos^2\alpha} + \frac{l_2^2}{\sin^2\alpha} + 2RC\right)\Phi_\mu(R;\Omega) = U_\mu(R)\Phi_\mu(R;\Omega) \tag{6}$$

and the hyperradial function $F(R)$ satisfies the coupled equations,

$$\left(\frac{d^2}{dR^2} + \frac{1}{4R^2} - U_\mu(R) + W_{\mu\mu}(R) + 2E_n\right)F^n_\mu(R) + \sum_\nu W_{\mu\nu}(R)F^n_\nu(R) = 0 \tag{7}$$

where the coupling terms W are defined as

$$W_{\mu\nu} = 2\left\langle\Phi_\mu\left|\frac{d}{dR}\right|\Phi_\nu\right\rangle\frac{d}{dR} + \left\langle\Phi_\mu\left|\frac{d^2}{dR^2}\right|\Phi_\nu\right\rangle \tag{8}$$

By dropping all the coupling terms and keeping only the diagonal terms, Eq. (7) becomes

$$\left(\frac{d^2}{dR^2} + \frac{1}{4R^2} - U_\mu(R) + W_{\mu\mu}(R) + 2E_n\right)F^n_\mu(R) = 0 \tag{9}$$

Notice that the second-order diagonal $W_{\mu\mu}(R)$ term is included in Eq. (9) as part of the effective potential. This term is usually excluded in the Born–Oppenheimer expansion in diatomic molecules, but it is included in the "adiabatic approximation"[3] of Eq. (9). Under this approximation, the wave function for the nth state within channel μ is given approximately by

$$\Psi^n_\mu(R,\Omega) = F^n_\mu(R)\Phi_\mu(R;\Omega)/(R^{5/2}\sin\alpha\cos\alpha) \tag{10}$$

The adiabatic approximation was first introduced by Macek (1968) to study doubly excited states of helium. The energy levels calculated from this approach were found to be in good agreement with experimental results and with other calculations. Later work was directed at understanding the correlation properties hidden in the "channel functions" $\Phi_\mu(R;\Omega)$. The major task

of understanding and classifying electron correlations is then to untangle this multivariable function in appropriate display and to sort out the order and regularities. To this end, sectional views of the channel function $\Phi_\mu(R;\Omega)$ on the relative angles α and θ_{12} are appropriate. We will proceed with simple examples and then to the complete spectra of doubly excited states. For simplicity, we will first consider $L = 0$ states only.

B. Angular Correlations

Angular correlation is quite familiar. The wave function for an $L = 0$ two-electron state has the general form

$$\psi(R,\alpha,\theta_{12}) = \sum_l \Phi_l(r_1,r_2)\mathcal{Y}_{l00}(\hat{r}_1,\hat{r}_2) \tag{11}$$

where

$$\mathcal{Y}_{l00} = (-1)^l\left(\frac{2l+1}{4\pi}\right)^{1/2}P_l(\cos\theta_{12}) \tag{12}$$

Therefore, if the two-electron state can be designated as s^2 or any linear combination of ss', there is no θ_{12} dependence in the wave function and there is no angular correlation between the two electrons. If it is designated as p^2 or pp', then the wave function is multiplied by an overall $\cos\theta_{12}$ factor. According to the traditional picture, correlation is defined as the deviation from the prediction of the independent particle approximation. Therefore, the angular correlation for a state designated by pp', for example, is defined to be the deviation of its wave function from the $\cos\theta_{12}$ dependence. We will not adopt this definition. Instead, we describe how electrons are correlated. Thus if the θ_{12} distribution of a given state is well described by $P_l(\cos\theta_{12})$, then that state can be designated by the independent particle notation l^2 or ll'. We will search for new designations for all doubly excited states where the independent particle approximation fails.

C. Radial Correlations

Similar to angular correlations, radial correlations are characterized by the distribution of the wave function in the hyperangle α. In the foregoing discussion, no distinction has been made between singlet and triplet states for angular correlations; their difference comes mostly in radial correlations. Radial correlation is less familiar. For the purpose of illustrating radial correlations, we examine the solution of the Schrödinger equation by neglecting the θ_{12} dependence in the potential. Under this approximation, l_1

and l_2 are good quantum numbers and states can be labeled as $1s^2$, $1s2s$, and $2s^2$, etc. If the wave functions are approximated as in Eq. (10), then these two variable functions can be displayed graphically.

In Fig. 4 we show the absolute value of the wave functions for $1s2s\ ^1S^e$, $2s^2\ ^1S^e$, and $2s3s\ ^1S^e$ (we use the independent-particle designation here) of He on the (r_1,r_2) plane. We notice that the $1s2s\ ^1S^e$ has a circular node, corresponding to R_0 = constant. The wave function for this state is concentrated in the region where $r_1 \ll r_2$ and in the region where $r_2 \ll r_1$ (by symmetry). In the $r_1 \ll r_2$ region, the wave function along r_2 for a given r_1 behaves like a hydrogenic $2s$ wave function. The wave function has noticeable amplitudes in the $r_1 = r_2$ region only when R is inside R_0. For $2s^2\ ^1S^e$, there are no circular nodes, but there are two radial nodal lines running almost parallel to the r_1 and the r_2 axes, each one corresponding to α = constant. For this state, the wave function has large amplitudes mostly in the region where $r_1 \approx r_2$. In this example, the $1s2s\ ^1S^e$ has a node in the hyperradial coordinate R and no node in the hyperangle α. For $2s^2\ ^1S^e$, there is no node in R but one node at α_0, where α_0 depends on R and lies between 0 and 45°. (By symmetry the other nodal line is given by $90° - \alpha_0$.) We can differentiate each state by the nature of its nodal lines. Let n_R and n_α denote the number of nodes in the wave function for the R $(0 < R < \infty)$ and α $(0 < \alpha < 45°)$ coordinates, respectively; then $1s2s\ ^1S^e$ has $(n_R,n_\alpha) = (1,0)$ while $2s^2\ ^1S^e$ has $(n_R,n_\alpha) = (0,1)$. The ground state, usually designated as $1s^2\ ^1S^e$, has $(n_R,n_\alpha) = (0,0)$. Using this notation, the $2s3s\ ^1S^e$ state has $(n_R,n_\alpha) = (1,1)$; so that this state has one node in R and one node in α. This is indeed the case, as shown in Fig. 4c.

So far we have discussed $^1S^e$ states only. Since the wave function for a $^1S^e$ state is symmetric under the interchange of the two electrons, the wave function is symmetric with respect to $\alpha = 45°$. For $^3S^e$ states, the wave function has a node at $\alpha = 45°$. This node is fixed at $\alpha = 45°$ and does not change with R. To account for the fact that the wave function is symmetric or antisymmetric with respect to $\alpha = 45°$, it is convenient to introduce a superscript A (= +1 or −1). The superscript A is not an independent quantum number, since $A = (-1)^S$ for $L = 0$ states; nevertheless it helps to bring out the symmetry property in the α coordinate with respect to $\alpha = 45°$. Thus all the ^1S states have the new designations of $(n_R,n_\alpha)^+$ and all $^3S^e$ states have $(n_R,n_\alpha)^-$ designations. Since $1s2s\ ^3S^e$ is the lowest $^3S^e$ states, it is given by $(0,0)^-$, indicating no node in R nor in α except for the fixed node at $\alpha = 45°$. In terms of the "total" number of nodal lines, both $1s2s\ ^1S^e$ and $1s2s\ ^3S^e$ states have one nodal line; the nodal line for the former is R = constant and for the latter is $\alpha = 45°$. From this, it is clear that $2s3s\ ^3S^e$ has the designation of $(0,1)^-$. In Fig. 5, we see that the corresponding density plot shows that the

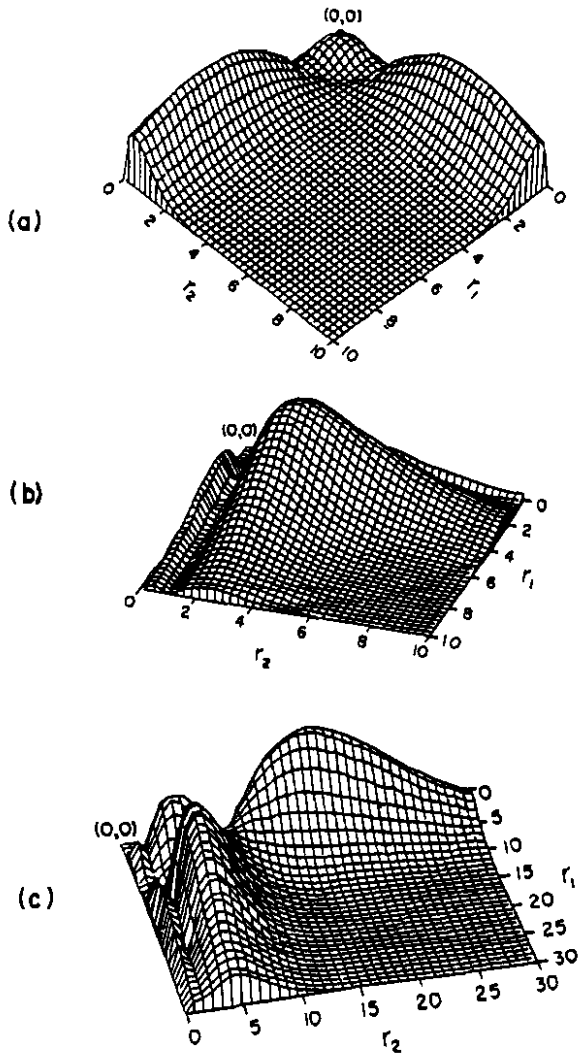

FIG. 4. Square root of the volume charge-density distribution of helium plotted in the (r_1,r_2) plane. The dependence of wave functions on θ_{12} has been neglected. (a) for $1s2s\ ^1S^e$; (b) $2s^2\ ^1S^e$; (c) $2s3s\ ^1S^e$.

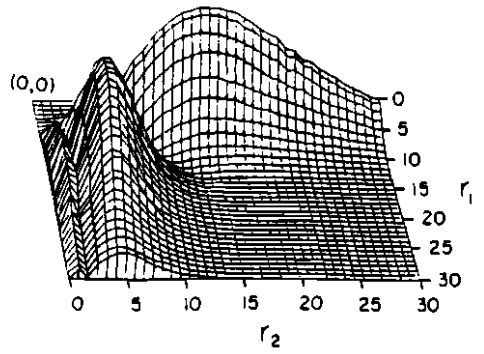

FIG. 5. Same as Fig. 4 except for the $2s3s\ ^3S^e$ of He.

number and nature of the nodal lines are consistent with the $(0,1)^-$ designation.

By neglecting the θ_{12} dependence in the potential, an $L \neq 0$ state can be expressed as

$$\psi_{l_1 l_2 LM} = F(R)[g(\alpha)\mathcal{Y}_{l_1 l_2 LM}(\hat{r}_1,\hat{r}_2) + (-1)^{l_1+l_2-L+S} g(\pi/2-\alpha)\mathcal{Y}_{l_2 l_1 LM}(\hat{r}_1,\hat{r}_2)] \quad (13)$$

in the quasiseparable approximation. In Eq. (13), the symmetry requirement with respect to the interchange of the two electrons does not impose any condition on the function $g(\alpha)$, since the symmetry is accounted for by the

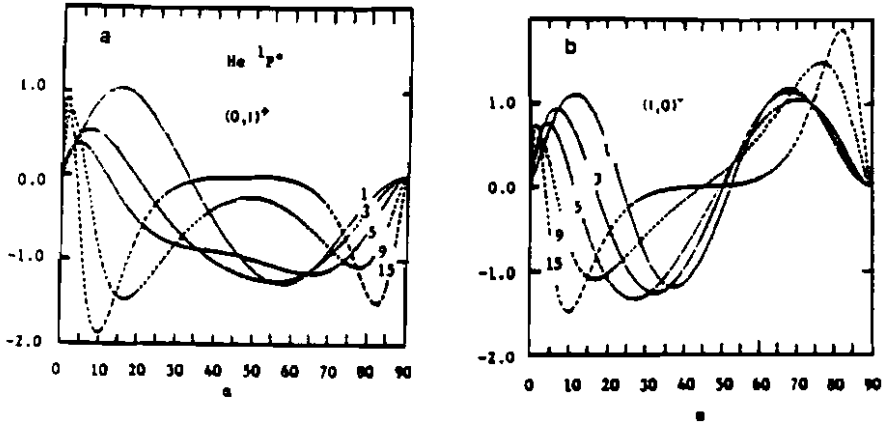

FIG. 6. Channel functions $g(\alpha;R)$ for the two $^{1,3}P^o$ channels of helium converging to the $N = 2$ limit of He^+. Shown are the $[l_1,l_2] = [0,1]$ components of each channel. The dipole component of the electron–electron interactions is neglected. (a) Shows $A = +1$ type behavior; (b) shows $A = -1$ type behavior in radial correlations.

second term on the right. States where the function $g(\alpha)$ itself does not have a well-defined or approximate nodal or antinodal structure at $\alpha = 45°$ are assigned $A = 0$. All singly excited $L \neq 0$ states have $A = 0$. For $L \neq 0$ doubly excited states, in addition to $A = 0$ channels, there are channels where $g(\alpha)$ exhibits near-antinodal or nodal structure at $\alpha = 45°$. These channels are classified with $A = +1$ and $A = -1$, respectively (Lin, 1974b). For example, the two $^{1,3}P^o$ channels of helium converging to the $N = 2$ limit of He^+ have these behaviors. By neglecting the θ_{12} dependence in the potential, we show in Fig. 6 the $[l_1,l_2] = [0,1]$ component of the channel functions. The upper figure shows approximately antinodal structure at $\alpha \approx 45°$, similar to the + channels. The lower figure shows an approximate node at an angle close to $\alpha = 45°$, similar to the − channels. This approximate +/− symmetry is one of the most striking features of doubly excited states.

D. Radial and Angular Correlations

In discussing radial correlations we purposely neglected angular correlations for simplicity. However, angular and radial correlations are not separable. Consider $L = 0$ states in the quasiseparable approximation: All the information about electron correlations is contained in the channel function $\Phi(R;\alpha,\theta_{12})$. To show the correlation pattern of two excited electrons, we exhibit the surface densities on the hyperspherical surface, $R(\Omega) =$ constant, by displaying plots of $|\Phi(R;\alpha,\theta_{12})|^2$ on the (α,θ_{12}) plane.

A few general remarks will be helpful in understanding the structure of the charge-density plots to be given below. All the channel functions solved from Eq. (6) at a given value of R are orthogonal, corresponding to the surface harmonics on the $R(\Omega) =$ constant surface. The higher harmonics are orthogonal to the lower ones with an increasing number of nodal lines on the (α,θ_{12}) plane. In Eq. (6), the channel function $\Phi(R;\alpha,\theta_{12})$ and the eigenvalue $U(R)$ depend not only on the kinetic energy operators, but also on the Coulomb interactions between the three charges. To avoid large kinetic energies, the channel functions must be smooth with respect to α and θ_{12} and possess few nodal lines. To achieve lower potential energies, the electron–nucleus interaction favors the small-α (or $\alpha = \pi/2$) region, while the electron–electron repulsion term favors the region where $\alpha = \pi/4$ and $\theta_{12} = \pi$. Thus the excitation energies $U(R)$ and the pattern of electron correlations are "decided" by these competing factors. The lowest channel is "allowed" to have all the favorable factors at a given R, while the higher channels approach these favorable factors under the constraint of orthogonality to the lower ones. These constraints and the nature of Coulomb potentials set up the pattern of electron correlations for doubly excited states.

We first illustrate how the correlation pattern for a given channel evolves as the hyperradius R changes. In Fig. 7 we show the potential curve $U(R)$ for the ground channel of H^- and the surface plots of $|\Phi(R;\alpha,\theta_{12})|^2$ for four values of R. At $R \approx 1$ and 2, the kinetic energy term, which is proportional to $1/R^2$, is large and the charge cloud spreads over the whole (α,θ_{12}) plane. Along the ridge, $\alpha = 45°$, the two electrons tend to stay closer to $\theta_{12} = 180°$. At larger R, $R = 4$ and 8, the potential energy term dominates so that the two electrons tend to stay near small α (or $\alpha = 90°$), where the electron–electron repulsion is small. Therefore the channel function becomes nearly independent of θ_{12}. This lack of angular correlation is quite evident in the density plot for $R = 8$.

To get an estimate of how important the angular or radial correlations are for a given state for this channel, it is necessary to consider the hyperradial wave function of that state. For example, if the state has large amplitudes in $F(R)$ for small R, then the angular correlation (or the deviation from the

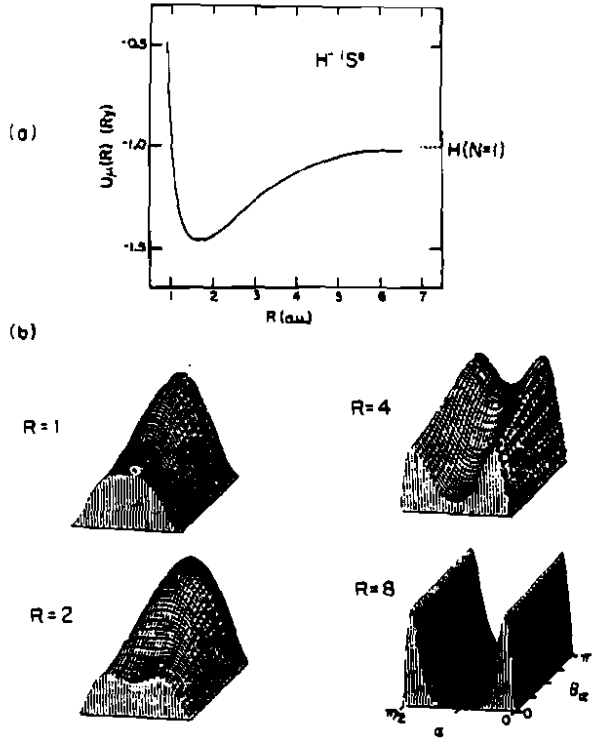

FIG. 7. (a) Hyperspherical potential curve for the ground $^1S^e$ channel of H^-. (b) Surface charge distribution for the $^1S^e$ ground channel of H^- plotted on the (α,θ_{12}) plane at selected values of R.

independent particle approximation) is large. If the amplitude $F(R)$ for the state is mostly in the large-R region, then there is little angular correlation, since in the large-R region the channel function is similar to that shown for the $R = 8$ plot, which shows little angular correlation.

We next discuss the correlations for the two $^1S^e$ doubly excited channels of H^- that converge to the $N = 2$ limit of H. The two potential curves are shown in Fig. 8a; they are labeled as $(1,0)^+$ and $(-1,0)^+$ channels. The labeling will be explained in the next section. For the moment we note that the $(1,0)^+$ channel has an attractive potential well while the $(-1,0)^+$ channel is completely repulsive. The surface charge-density plots for the two channels are given in Fig. 8b at $R = 8$, 12, 20. It is obvious that the correlation patterns for the two channels are quite different. They are also quite different from the

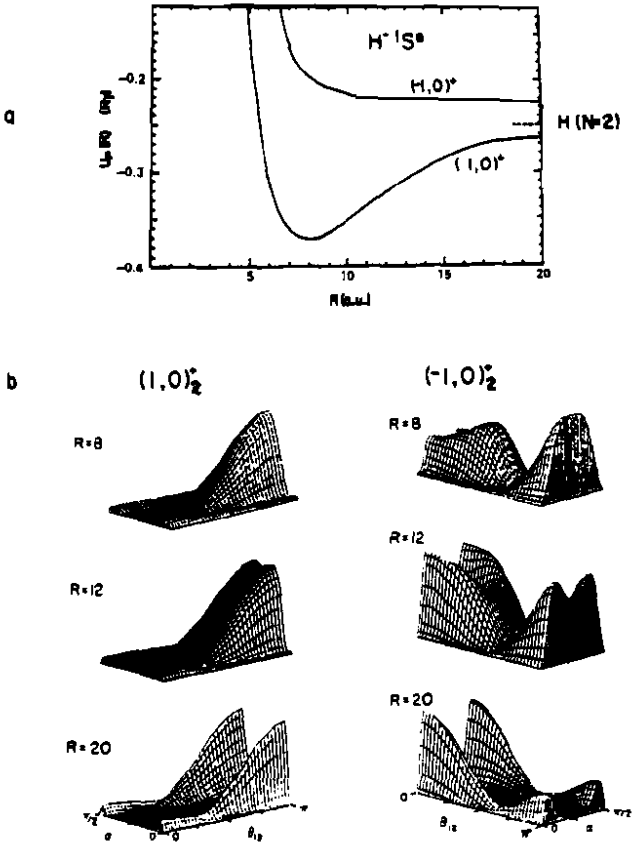

FIG. 8. (a) Hyperspherical potential curves for the two $^1S^e$ channels which converge to the $N = 2$ of H. (b) Surface charge-density plots for the two channels at the values of R shown. Note the difference in the orientation of the figures along the two columns.

ground channel shown in Fig. 7. The $(1,0)^+$ channel has large charge densities in the large-θ_{12} region; it also has a nodal line near small α (and, by symmetry, another one near $\alpha = 90°$). For a given value of R, say $R = 8$, when the ground channel occupies the small-α region (and the $\alpha = 90°$ region), its amplitudes are vanishingly small in the $\alpha \sim 45°$ region. At this same value of R, we notice that the $(1,0)^+$ channel occupies most of the large-θ_{12} region of the (α,θ_{12}) plane not occupied by the $(0,0)^+$ channel. By concentrating the charge distribution in the $\alpha \sim 45°$ and large-θ_{12} region, the $(1,0)^+$ channel minimizes the kinetic energy and the electron–electron repulsion. The repulsive $(-1,0)^+$ channel exhibits charge distribution mostly in the $0 < \theta_{12} < 90°$ region. The two electrons tend to stay on the same side of the nucleus and thus experience a large electron–electron repulsion. This region, however, is still preferable under the circumstances. Forcing the two electrons to the large-θ_{12} region would require additional nodal lines, which would increase the expectation value of the kinetic energy and the excitation energy $U(R)$.

As R increases, we notice that the major change in the channel density plots is that the density in the middle $\alpha \simeq 45°$ region drops while the θ_{12} dependence remains nearly constant. The drop in the $\alpha \simeq 45°$ region occurs when the two electrons in that channel become confined in the two potential valleys. With this type of R dependence in mind, we can now look at the correlations of higher channels for a given value of R only. In Fig. 9 we show the charge-density plots at $R = 20$ for the three $^1S^e$ doubly excited channels of H^- that converge to the $N = 3$ limit of H. The three channels are labeled $(2,0)^+$, $(0,0)^+$, and $(-2,0)^+$. We note that the charge-density distribution for the $(2.0)^+$ channel is quite similar to that for the $(1,0)^+$ channel shown in Fig. 8b except that the $(2,0)^+$ channel has a sharper structure around the Wannier point ($\theta = 45°$ and $\theta_{12} = 180°$). The $(0,0)^+$ channel has a pronounced peak near $\theta_{12} = 90°$, in addition to some density in the large-θ_{12} region. The $(-2.0)^+$ channel is marked by a large charge density in the small-θ_{12} region.

One can continue this type of display for doubly excited states that converge to the higher channels. It is obvious, however, that among the channels that converge to a given hydrogenic N limit, the charge density for the lowest channel tends to peak at $\theta_{12} = 180°$, while the highest (or the most repulsive) one tends to peak near $\theta_{12} = 0$ and the intermediate channels occupy the intermediate-θ_{12} region. Physically this means that the most energetically stable state is the one where the two electrons are on opposite sides of the nucleus.

Our discussions so far in this subsection have dealt with $^1S^e$ states only. The different channels presented differ only in their angular correlations. For $^3S^e$ states, the lowest channel is labeled $(0,0)^-$, the two channels that converge to the $N = 2$ of H are $(1,0)^-$ and $(-1,0)^-$, and the three channels

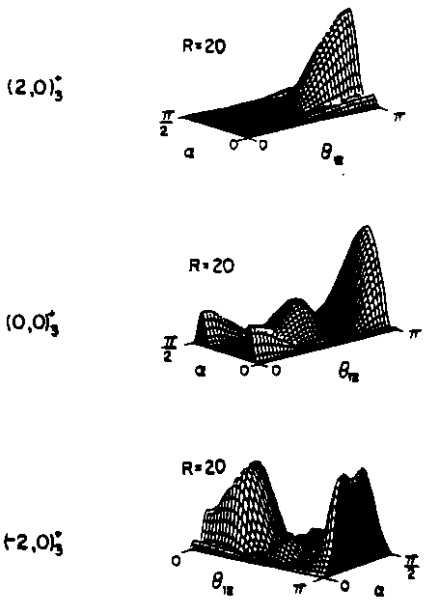

FIG. 9. Surface-density plots at $R = 20$ for the three $^1S^e$ channels of H^- converging to the $N = 3$ limit of H. Note the difference in the orientation of the last figure.

that converge to the $N = 3$ of H are $(2,0)^-$, $(0,0)^-$, and $(-2,0)^-$. The difference between the corresponding $^1S^e$ and $^3S^e$ channels is in the radial correlation. For $^3S^e$ channels the symmetry condition is such that the charge density has to vanish at $\alpha = 45°$. Thus, for example, the $(1,0)^+$ $^1S^e$ and $(1,0)^-$ $^3S^e$ channels have a similar θ_{12} dependence; i.e., they have similar angular correlations, but different radial correlations; the wave function at $\alpha = 45°$ is an antinode for $^1S^e$ and a node for $^3S^e$ (Lin, 1982a).

E. The Validity of the Quasiseparable Approximation

At this point we will make a short diversion to discuss the question of the validity of the adiabatic approximation (Lin, 1983a), which was used in the study of doubly excited states in hyperspherical coordinates. In the conventional Born–Oppenheimer approximation for diatomic molecules, quasiseparability was often attributed to the small ratio of the electron mass to the mass of the nuclei. The corresponding ratio in two-electron problems is unity. Therefore it is not obvious why one can use the quasiseparable approximation.

We emphasize that the reason for the validity of the quasiseparable ap-

proximation is dynamical in origin. It is due to the large difference in the quantization energies along different coordinates. This quasiseparability is independent of the choice of hyperangles and is not limited to two-electron problems. In recent years, it has been established that many atomic and molecular problems can be solved in the quasiseparable approximation if the problems are expressed in hyperspherical coordinates (Lin, 1986; Manz, 1985).

For two-electron problems, it is possible to check if the wave functions calculated using different approaches resemble those calculated using hyperspherical coordinates in the adiabatic approximation. This has been examined for the configuration-interaction (CI) wave functions of Lipsky *et al.* (1977). (See Lin, 1983a.) If we rewrite the $^{1,3}S^e$ CI wave function $\psi(\mathbf{r}_1,\mathbf{r}_2)$ in hyperspherical coordinates, then

$$\psi(\mathbf{r}_1,\mathbf{r}_2) = F_n(R)\Phi_\mu^n(R;\alpha,\theta_{12}) \tag{14}$$

where state n belongs to channel μ. In Eq. (14), $\Phi_\mu^n(R;\alpha,\theta_{12})$ is normalized on the surface at R = constant. From the known CI wave functions, both $F_n(R)$ and $\Phi_\mu^n(R;\alpha,\theta_{12})$ can be determined. Here we consider the three lowest $^1S^e$ states of helium belonging to the $(1,0)^+$ $^1S^e$ channel, which lies below the He^+ ($N = 2$) limit. The hyperradial functions deduced from Eq. (14) are shown in Fig. 10. These functions behave as expected: The lowest state does not have any node in R, while each higher state acquires one more node in R. In Eq. (14), our notation indicates that we do not assume that $\Phi_\mu^n(R;\alpha,\theta_{12})$ is independent of n. In the quasiseparable approximation in hyperspherical coordinates, as indicated in Eq. (10), each wave function is given by $F_n(R)\Phi_\mu^{adi}(R;\alpha,\theta_{12})$. We can calculate the overlap integral

$$I = \langle \Phi_\mu^n(R;\alpha,\theta_{12}) | \Phi_\mu^{adi}(R;\alpha,\theta_{12}) \rangle \tag{15}$$

as a function of R to determine the region where the two functions differ. We indicate the results in Fig. 10. If the overlap [Eq. (15)] is larger than 95% in that region of R, the curves are shown in solid lines. If the overlap is less than 95%, the curves are shown in dashed lines. From Fig. 10 we notice that the overlap is larger than 95% in the region where the hyperradial function $F(R)$ is larger. This clearly illustrates that wave functions calculated from other approaches, when expressed in hyperspherical coordinates, also exhibit quasiseparability in the region where the charge density is large.

We can also display the correlation patterns of wave functions calculated using other approaches using the conversion equation [Eq. (14)]. In Fig. 11, we show the surface charge densities of the lowest state of each of the $(2,0)^+$, $(0,0)^+$, and $(-2,0)^+$ $^1S^e$ channels of He which lie below the He^+ ($N = 3$) limit calculated using the CI method (Lipsky *et al.*, 1977). These surface plots are quite similar to those shown in Fig. 9 for H^-.

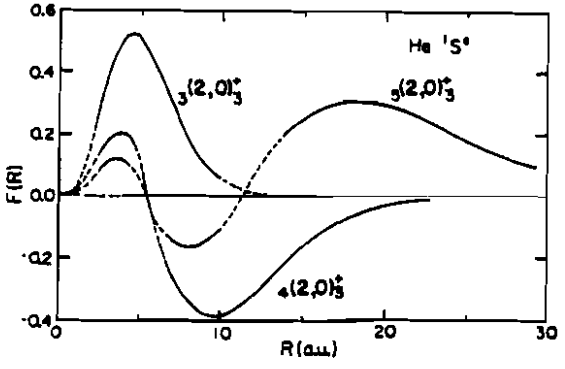

FIG. 10. R-weighted hyperradial wave functions of the three lowest CI states of the $(1,0)^+_3$ $^1S^e$ series of helium below the $N = 2$ limit of He^+. The curves are shown in solid lines in regions where the angular part of the CI wave function has a large overlap integral (>95%) with the adiabatic channel function. In regions of R where the overlap is less than 95%, the curves are shown as dashed lines.

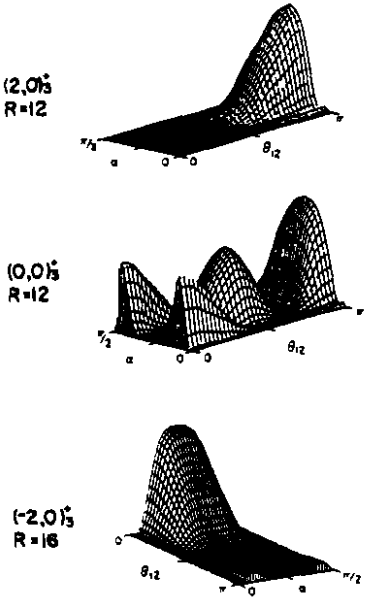

FIG. 11. Surface-density plots for the lowest states of each of the three $^1S^e$ Rydberg series of helium calculated from the CI approximation. These plots are similar to those shown in Fig. 9, which were calculated using the adiabatic approximation.

III. Classification of Doubly Excited States

In this section we shall describe the classification of doubly excited states in terms of a set of correlation quantum numbers, K, T, and A. The enumeration of these quantum numbers and their approximate physical meaning will be given. A more precise mathematical definition of these correlation quantum numbers will be postponed until Section V. Surface charge-density plots will be used to help visualize the correlation patterns described by these quantum numbers. It will then be shown that states having identical correlation quantum numbers have isomorphic correlations. This isomorphism is the underlying reason for the existence of supermultiplet structure of doubly excited states. The last subsection discusses how the independent electron picture fits into the present classification scheme.

A. The Classification Scheme

In the present scheme, a given state of a two-electron atom is designated by the notation ${}_n(K,T)_N^A\ {}^{2S+1}L^\pi$, where L, S, and π are the usual quantum numbers, N is the principal quantum number of the inner electron, and n is the principal quantum number of the outer electron. The spin-orbit interaction is not considered throughout our discussion but can be easily included in a perturbative treatment. A given channel or a Rydberg series μ is described by the notation $\mu = (K,T)_N^A\ {}^{2S+1}L^\pi$. Here the principal quantum number N denotes the hydrogenic principal quantum number in the dissociation limit. The rules for the assignment of K, T, A, and n for a given L, S, N, and π are discussed below.

1. Assignment of K and T

Following Herrick and Sinanoglu (1975), the possible values of K and T for a given N, L, and π are determined by

$$\begin{aligned} &T = 0, 1, 2, \ldots, \min(L, N-1) \\ &K = N-1-T, N-3-T, \ldots, -(N-1-T) \end{aligned} \tag{16}$$

For states where $\pi = (-1)^{L+1}$, $T = 0$ is not allowed. Notice that the assigned values of K and T do not depend on S. Roughly speaking, T is the projection of the total angular momentum L onto the interelectronic axis and

$$K \approx -(r_< \cos\theta_{12}) \tag{17}$$

where $r_<$ is the radius of the inner electron. These two quantum numbers K and T were originally used by Herrick and Sinanoglu (1975a,b) to characterize approximate doubly excited state wave functions for intrashell states. Based upon a group-theoretical analysis, they showed that the configuration-interaction wave functions for doubly excited states can be approximated by "doubly excited symmetry basis" (DESB) functions. The validity and the limitation of DESB functions for representing doubly excited states were examined by Lin and Macek (1984).

2. Assignment of A

This radial correlation quantum number A was supplemented to emphasize the radial correlation of the two electrons (Lin, 1983d, 1984). Its meaning has been illustrated in Section II,C in connection with the model problem, where angular correlation was neglected. The quantum number A can take values of $+1$, -1, and 0 only. Both $A = +1$ and -1 states can have large amplitudes on the potential ridge. We stress that the $A = +1$ channel has an antinodal structure at or near $\alpha = \pi/4$ (this statement will be made more precise in Section V), while the $A = -1$ channel has a node at or near $\alpha = \pi/4$. Electrons in the $A = 0$ states are confined in the two potential valleys. These states are similar to singly excited states.

The radial correlation quantum number A is not independent of K and T for a given L, S, N, and π. It is given by the following simple relations (Rau, 1984)

$$\begin{aligned} &A = \pi(-1)^{S+T} = \pi(-1)^{S+N-K+1} && \text{if } K > L-N \\ &A = 0 && \text{if } K \leqslant L-N \end{aligned} \tag{18}$$

With the relations in Eqs. (16) and (18), all the correlation quantum numbers K, T, and A for states converging to a hydrogenic limit N can be assigned. For $L \geqslant 2N-1$, all the channels have $A = 0$.

In terms of these correlation quantum numbers, K, T, and A, all the doubly excited states of two-electron atoms can be uniquely designated. From the correlations characterized by these quantum numbers, it is possible to understand the photoabsorption data systematically.

3. Selection Rules for Photoabsorption

According to the present recommended notation, the three ${}^1P^0$ Rydberg series of He below the $N = 2$ limit of He^+ are $(0,1)_2^+$, $(1,0)_2^-$, and $(-1,0)_2^e$. They are to replace the $2snp + 2pns$, $2snp - 2pns$, and $2pnd$ notations used by Cooper *et al.* (1963). The designations of Cooper *et al.* emphasize radial correlations only and cannot be generalized to other doubly excited states.

From the meaning of the correlation quantum numbers, one can deduce from the notation that for states belonging to the $(0,1)_2^+$ channel, the inter-electronic angle θ_{12} is nearly 90°, and the two electrons have in-phase radial oscillations, meaning that both electrons approach or leave the small-R region simultaneously. For states belonging to the $(1,0)_2^-$ channel, the two electrons are on opposite sides of the nucleus with large probabilities near $\theta_{12} = 180°$, but they have out-of-phase radial oscillations, meaning that when one electron is approaching the nucleus the other is moving away from the nucleus. For states belonging to the $(-1,0)_2^e$ channel, the two electrons are confined in the potential valleys; there is no radial correlation although the two electrons tend to stay on the same side of the nucleus.

The first photoabsorption data for the excitation of helium doubly excited states (Madden and Codling, 1963, 1965) indicated that only the $(0,1)_2^+$ channel is prominently excited, the $(1,0)_2^-$ channel is barely visible, and the $(-1,0)_2^e$ channel is completely absent. From the data of Woodruff and Samson (1982), as shown in Fig. 1, the prominent series below each of the $N = 3$, 4, and 5 series, respectively, are the $(1,1)_3^+$, $(2,1)_4^+$, and $(3,1)_5^+$ channels. There are some indications that the $(-1,1)_3^+$ and $(0,1)_4^+$ channels are also slightly populated. Since the ground state of He belongs to the $(0,0)_1^+$ channel, these experimental data indicate that the selection rule for photoabsorption is $\Delta A = 0$ and $\Delta T = 1$, and the most probable K for a given N is the maximum K for the allowed $T = 1$, i.e., $K = N - 2$.

4. *Assignment of n*

To be consistent with the principal quantum numbers used in the independent particle model, the smallest principal quantum number n_{min} of the outer electron is chosen as follows.

(a) The lowest n for all $A = +1$ channels is $n_{min} = N$.
(b) The lowest n for all $A = -1$ channels is $n_{min} = N + 1$.
(c) The lowest n for the lowest $A = 0$ channel is $n_{min} = N + 1$, and successive higher $A = 0$ channels have n_{min} increases by one unit for each $\Delta K = -1$. Channels having identical K but different T have the same n_{min}.

According to these rules, all intrashell states have $A = +1$ with $n = N$. The lowest doubly excited states for each of the five $^1P^o$ channels below $N = 3$ are ${}_3(1,1)_3^+$, ${}_4(2,0)_3^-$, ${}_3(-1,1)_3^+$, ${}_4(0,0)_3^-$, and ${}_4(-2,0)_3^e$. These rules also apply to high-angular-momentum states where all the states belong to $A = 0$. For example, the six channels for $^{1,3}H^o$ have the following lowest states: ${}_4(2,0)_3^e$, ${}_5(1,1)_3^e$, ${}_6(0,2)_3^e$, ${}_6(0,0)_3^e$, ${}_7(-1,1)_3^e$, and ${}_8(-2,0)_3^e$. Recall that these states are $3s6h$, $3p5g$, $3p7i$, $3d4f$, $3d6h$, and $3d8j$, according to the independent particle picture. Therefore, the lowest n's are 4, 5, 6, 6, 7, and 8, as predicted by

rule (c) above. The $(K,T)^A$ designation is preferable to the independent particle notation even for the $A = 0$ states because it provides information about angular correlations; there is no such information available in the independent particle description. The number of nodes in the hyperradial function $F(R)$ for a given n of the outer electron is given by $n - n_{min}$, where n_{min} is the minimum n of the given channel.

B. Potential Curves

In the quasiseparable approximation in hyperspherical coordinates, the wave functions are given by $F_\mu^n(R)\Phi_\mu(R;\Omega)$. The channel function $\Phi_\mu(R;\Omega)$ contains information about electron correlations, which is reflected in the shape of the channel potential $U(R)$. Now that the channels are identified by $\mu = (K,T)_N^{A\,2S+1}L^\pi$, channels with identical correlation quantum numbers K, T, and A should have nearly identical correlation patterns and nearly identical potential curves if the correlation determines predominantly the energies of the channel. In this subsection, we discuss the potential curves.

In Fig. 12 we show the potential curves of He $^{1,3}S^e$, $^{1,3}P^o$, and $^{1,3}D^e$ that converge to the $He^+(N = 3)$ limits. Similar curves for higher L's are shown in Fig. 13. Only channels that have $\pi = (-1)^L$ are shown. Each potential curve

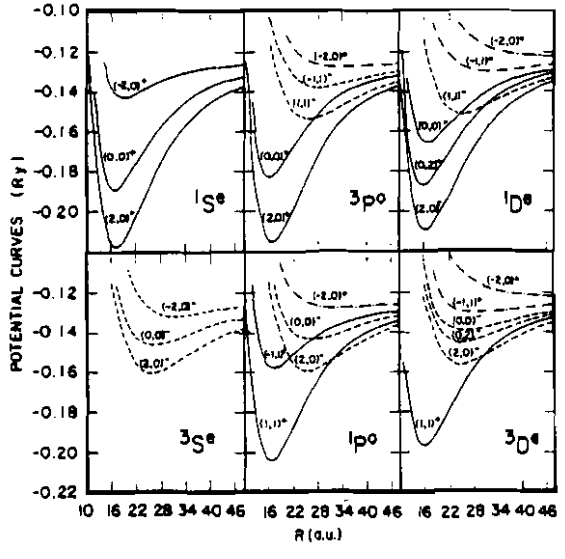

FIG. 12. Potential curves for all the $^{1,3}S^e$, $^{1,3}P^o$, $^{1,3}D^e$ channels for He that converge to $He^+(N = 3)$. Curves are labeled in terms of K, T, and A correlation quantum numbers. Reduced units with $Z = 1$ are used.

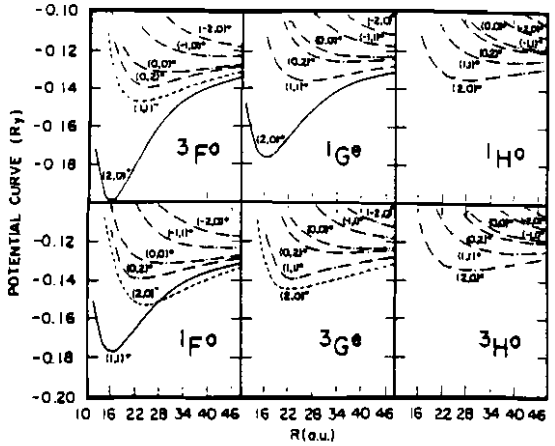

FIG. 13. Same as in Fig. 12 except for $^{1,3}F^0$, $^{1,3}G^e$, and $^{1,3}H^0$ channels.

is labeled with K, T, and A quantum numbers. We first note that curves which have identical K, T, and A quantum numbers are quite similar and are nearly degenerate. (All the calculations for He are done using reduced units with $Z = 1$.)

The assignment of correlation quantum numbers for each manifold follows these rules:

(1) For a given L, S, π, and N, find the allowed combinations of $(K,T)^A$ from Eqs. (16) and (18).

(2) Order the asymptotic potential curves from the bottom starting with the maximum allowable K and then in order of decreasing K. If there is more than one values of T for a given K, order from below according to decreasing values of T.

(3) At small R, the lower or the more attractive curves belong to the $A = +1$ channels. Among the + channels, the large K goes with the lower curve and for a given K, the larger T with the lower curve. First all the $A = +1$ curves are assigned, then the $A = -1$ channels, and last the $A = 0$ using the same rule for each A group.

(4) Connect curves with identical K and T in the two regions. Only the + and − curves are allowed to cross.

The possible number of channels of doubly excited states for states converging to higher $He^+(N)$ limits is quite numerous. As an illustration, we show in Fig. 14 the potential curves of $^{1,3}S^e$, $^{1,3}P^0$, $^{1,3}D^e$, and $^{1,3}F^0$ states of He below the $He^+(N = 4)$ limits. There are 4, 7, 9, and 10 channels for $L = 0$, 1, 2, and 3, respectively. The correlation rules discussed above can be used to construct the "diabatic" curves shown. Notice that the + curves are distinctly more attractive and are capable of supporting low-lying bound states. Experimental data on these high-lying doubly excited states are very scarce.

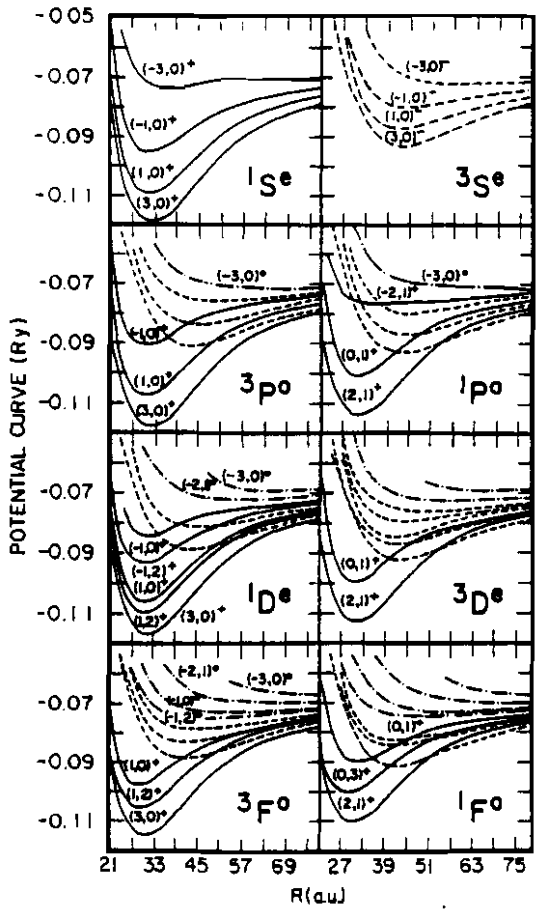

FIG. 14. Same as in Fig. 12 except for the $^{1,3}S^e$, $^{1,3}P^0$, $^{1,3}D^e$, and $^{1,3}F^0$ channels that converge to the $N = 4$ limit of He^+. (———) The + channels; (– – –) the − channels; and (— · —) the $A = 0$ channels. Labels for all the + channels are indicated. The K and T quantum numbers for − channels for singlets are obtained from the K and T of + channels of triplets, and vice versa. The K and T of $A = 0$ channels are the same for singlet and triplet.

The correlation rules presented here can be understood more rigorously in a later analysis (see Section V). Qualitatively, at large R, the electrons for all states are confined to the potential valleys where radial correlation is not important so the ordering of potentials at large R is independent of A. If the state has a large K, the angle θ_{12} between the two electrons is large, producing a smaller electron – electron repulsion which in turn results in lower $U(R)$. At

small R, radial correlation is more important. Channels that have antinodal structure at $\alpha = \pi/4$ have lower $U(R)$. For a given A, a large K again relates to smaller electron–electron repulsion and thus lower $U(R)$. The crossing between + and − channels is due to the change of the relative importance of radial and angular correlations as R changes.

C. Correlation Patterns and Isomorphism

To display the correlated motion of two electrons in a given channel, we have to exhibit the surface charge distribution $|\Phi_\mu(R;\Omega)|^2$ of the channel functions, similar to those shown in Figs. 7–9. For $L \neq 0$ channels, the channel functions depend on five angles, but three of these angles describe the rotation of the whole atom. To exhibit the internal correlation structure, we calculate the averaged surface charge densities (Warner, 1980; Ezra and Berry, 1982; Lin, 1984)

$$\sigma_\mu(R;\alpha,\theta_{12}) = \langle \Phi_\mu(R;\Omega') | \delta(\alpha' - \alpha)\, \delta(\cos\theta'_{12} - \cos\theta_{12}) | \Phi_\mu(R;\Omega') \rangle \quad (19)$$

The explicit expression of σ_μ was given in Appendix A of Lin (1984). With the definition of averaged surface charge density given by Eq. (19), we can now display the correlated motion of any two-electron channel functions for arbitrary L, S, and π. Channels which have identical correlation quantum numbers have isomorphic correlation patterns. To show this, we display in Fig. 15 and $(2,0)_3^+$ channel for $^1S^e$, $^3P^o$, $^1D^e$, and $^3F^o$ at $R = 20$. Referring to Figs. 12 and 13, at this value of R the potential for each channel is near the minimum. From Fig. 15, it is obvious that the correlation patterns for all

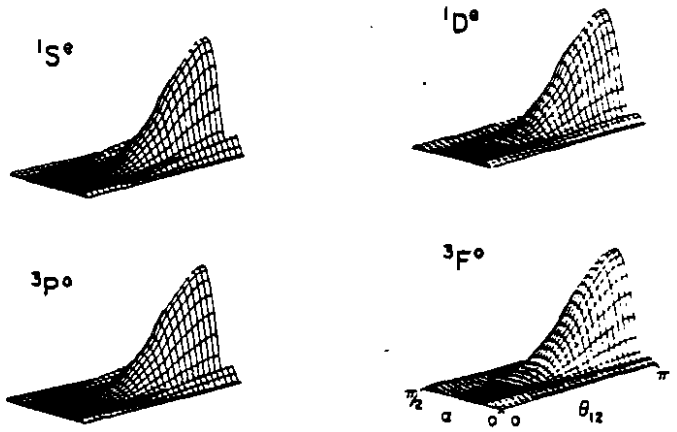

Fig. 15. Surface charge-density plots for the $(2,0)_3^+$ channels of $^1S^e$, $^3P^o$, $^1D^e$, and $^3F^o$ of He at $R = 20$.

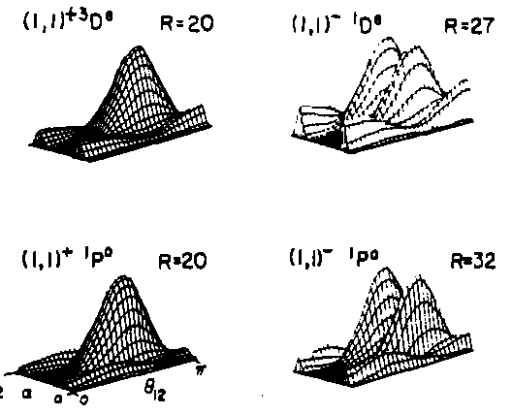

Fig. 16. Surface charge-density plots for the $(1,1)_3^+ {}^3D^e$, $(1,1)_3^- {}^1D^e$, $(1,1)_3^+ {}^1P^o$, and $(1,1)_3^- {}^3P^o$ at the values of R indicated. Notice that all four plots have similar θ_{12} dependence as the K and T quantum numbers are identical. The $A = +$ and $A = -$ channels differ in the nodal structure at $\alpha = \pi/4$.

these four channels are quite similar. They all exhibit a peak at $\alpha = 45°$, $\theta_{12} = 180°$, with little charge concentration for $\theta_{12} < 90°$. The difference is mostly in the region of small α (and $\alpha = \pi/2$). Further remarks on the origin of the difference will be given in Section V,C. We note that for a given N, channels which have $K = N - 1$ always have maximum densities in θ_{12} at $\theta_{12} = 180°$.

In Fig. 16 we show two more examples of isomorphism. The correlation patterns of $(1,1)_3^+ {}^3D^e$, $(1,1)_3^+ {}^1P^o$, $(1,1)_3^- {}^1D^e$, and $(1,1)_3^- {}^3P^o$ are displayed at the values of R given. The angle θ_{12} where the density is maximum occurs at $\theta_{12} \approx 120°$. The nodal structure near $\alpha = 45°$ for each channel is consistent with the + or − values assigned for the quantum number A for that channel. Since the K and T are identical for all these channels, we note that the θ_{12} distribution is identical for all of them.

Surface plots for other values of K, T, and A can also be pictured. As the value of K decreases, the charge distribution shifts toward the smaller θ_{12} region. For negative values of K, the two electrons are mostly on the same side of the nucleus. The surface plots of $A = +1$ channels have antinodal structure and the $A = -1$ channels have a fixed nodal line at $\alpha = 45°$. In $A = 0$ channels the two electrons never reach the potential ridge region.

D. Supermultiplet Structure

According to the quasiseparable approximation in Eq. (10) for the solution of the two-electron wave functions, the approximate energy eigenvalues

for a given channel μ are obtained by solving the one-dimensional equation [Eq. (9)] with the channel potential $U(R)$. Channels that have identical correlation quantum numbers $(K,T)^A$ but different L, S, and π, as we have shown in Section III,B, have nearly degenerate potential curves. This near-degeneracy in $U_\mu(R)$ gives near-degenerate eigenenergies. Thus doubly excited states exhibit new spectroscopic regularities if the energies are ordered according to correlation quantum numbers. This regularity was first discovered by Herrick and coworkers for intrashell doubly excited states from a group-theoretical analysis. It can be interpreted in terms of the moleculelike rovibrational modes. We will come back to this interpretation in Section V.

In Fig. 17 we plot the effective principal quantum number n^* of He^{**} below the $He^+(N=3)$ limits versus the correlation quantum numbers, $(K,T)^A$. The + and − states are grouped separately. Two new spectral regularities are obvious:

(1) The rotorlike structure of states which have the same $(K,T)^A$ but different L, S, and π. The "string" for each rotorlike series is determined from Eqs. (16) and (18). For a given K, T, and N, the allowed values of L for a rotor series is $L = T, T+1, \ldots, K+N-1$. Whether the rotor series is a + or a − series is determined by Eq. (18). There are situations where the number of states in a given string is small. For example, there is only one member for each of the $(0,2)_3^+\ ^1D^e$, $(-1,1)_3^+\ ^1P^0$, and $(-2,0)_3^+\ ^1S^e$ series.

(2) There is a repetition of $(K,T)^+$ and $(K,T)^-$ rotor structure. The − rotor series for a given $(K,T)^-$ can be obtained from the $(K,T)^+$ rotor series simply by interchanging the spins.

The energy levels shown in Fig. 17 were taken from the extensive CI calculation of Lipsky *et al.* (1977). These authors have classified the levels into different series according to the calculated quantum defects. Some of their assigned classifications were changed in order to preserve the regular rotor structure shown.

In Fig. 17 we also notice that states which have identical K, T, A, N, and L but different S and π are nearly degenerate. The small splitting is called T doubling. We notice that the $\pi = (-1)^{L+1}$ state always has slightly lower energy. The origin of this behavior will be explained in Section V,F.

Doubly excited states that converge to the higher thresholds exhibit more pronounced rotor structure. As an example, we display in Fig. 18 the energy levels of H^{-**} that lie below the $H(N=5)$ thresholds. These data were taken from the calculations of Ho and Callaway (1983). By assigning $(K,T)^+$ quantum numbers to these states and ordering the states according to the $(K,T)^+$ quantum numbers, the energies of these intrashell states are seen to exhibit rotorlike structure. The length of each "string" is much longer in this example. In fact, some higher members of the group have not been calculated.

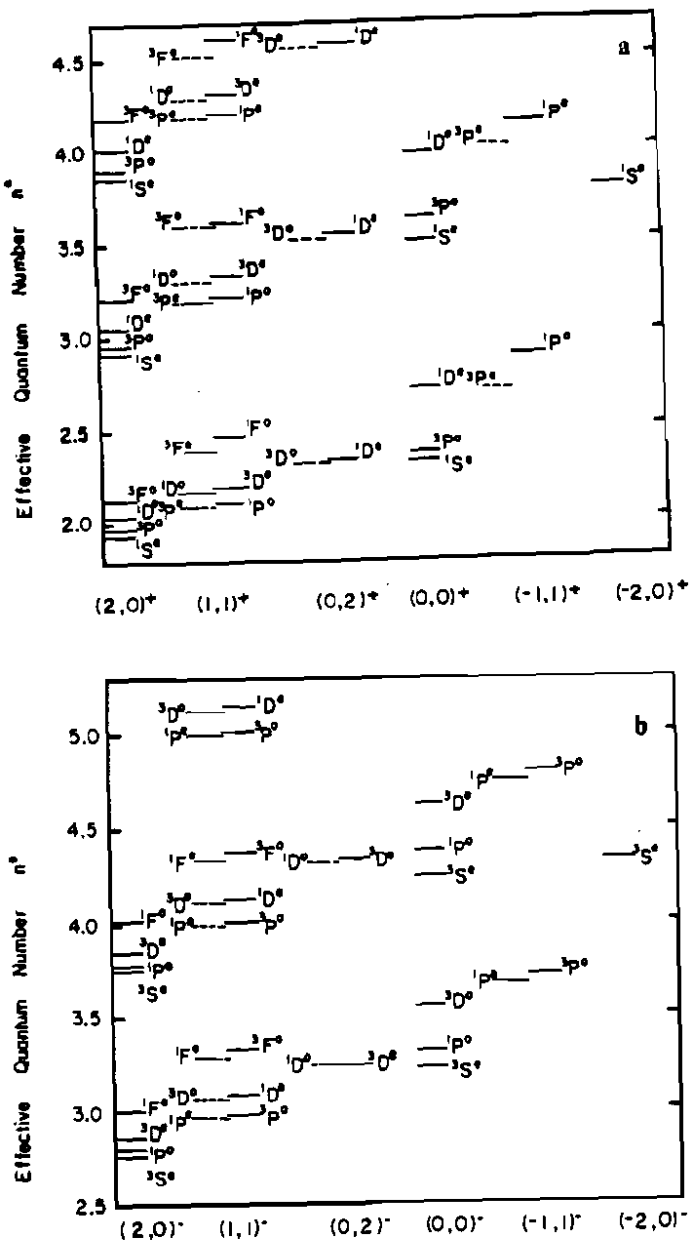

FIG. 17. Effective quantum number n^* grouped according to the (a) $(K,T)^+$ and (b) $(K,T)^-$ quantum numbers for doubly excited states of helium below the $He^+(N=3)$ limit. The rotorlike structure is evident for each given $(K,T)^+$ and $(K,T)^-$. Energy levels are taken from the calculation of Lipsky *et al.* (1977).

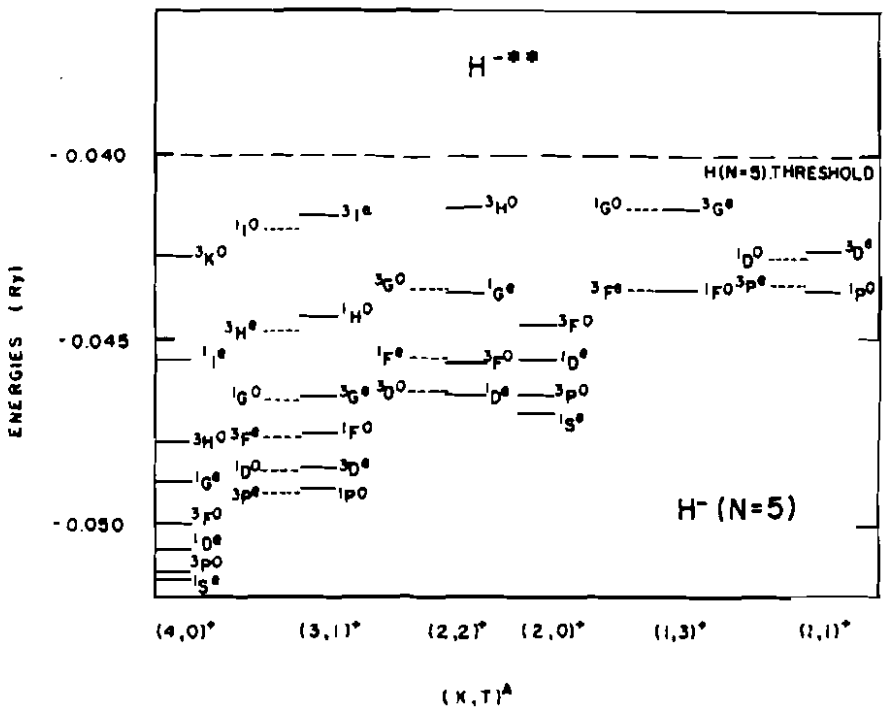

FIG. 18. Energy levels of H^- resonances lying below the H($N = 5$) limit of hydrogen grouped according to the $(K,T)^+$ quantum numbers. Data from Ho and Callaway (1983).

We must emphasize that the rotorlike structure applies to $A = +1$ and -1 channels only, but the T doubling applies to $A = 0$ channels as well.

E. Singly Excited States and Doubly Excited States with $A = 0$

The classification scheme discussed here applies to all states of two-electron atoms. It incorporates singly excited states as a subset. All singly excited states have $(K,T) = (0,0)$. For $^1S^e$, $A = +1$, for $^3S^e$, $A = -1$, and all of the other L's have $A = 0$. According to the independent-particle model, the energy for $1snL\ ^3L$ is always lower than the energy for $1snL\ ^1L$ for two-electron atoms. This is understood in terms of Pauli exchange correlations: In triplet states, the two electrons have parallel spins and thus they tend to stay away from each other spatially, thus reducing the electron–electron repulsion energy. From the hyperspherical viewpoint, this Pauli exchange correlation is reflected in the difference in angular correlation between the two electrons. To illustrate this point, the surface charge density plots for ^1P and ^3P are shown in Fig. 19 for three values of R. At large R, say $R = 6$, there is no evidence of angular correlation, and the charge distributions for singlet and triplet are identical. At smaller R, say $R = 2$, we notice that the triplet state has large charge concentration near $\theta_{12} = 180°$ while the singlet has larger concentration in the small-θ_{12} region. Thus the Pauli exchange correlation in the independent-electron picture is reflected in terms of angular correlations if it is visualized from the hyperspherical viewpoint.

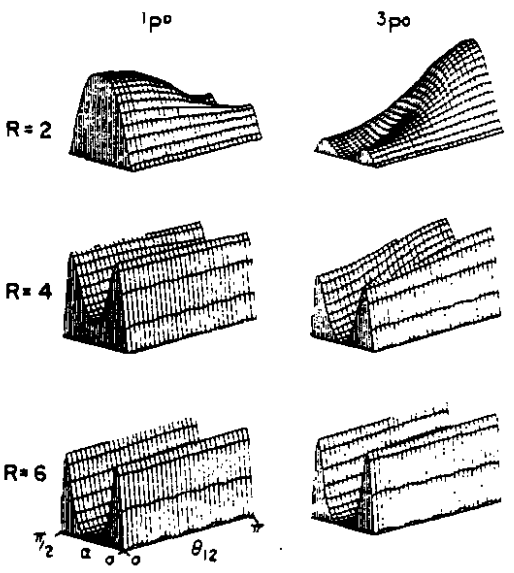

FIG. 19. Surface charge-density plots for the $1snp\ ^1P^0$ and $1snp\ ^3P^0$ channels of He at $R = 2$, 4, and 6. Notice that the Pauli exchange correlation is reflected as angular correlation in charge-density distributions.

The $A = 0$ states were mentioned earlier to be states where the electrons reside in the two potential valleys. In this respect, they are similar to singly excited states. In fact, their spectral behaviors do resemble those of singly excited states, as shown in Fig. 20. By displaying these states according to $(K,T)^0$, we notice that the triplet state in each case does lie lower in energy than the corresponding singlet state except in cases where the irregularity may be due to the numerical inaccuracy. Data were taken from Lipsky *et al.* (1977).

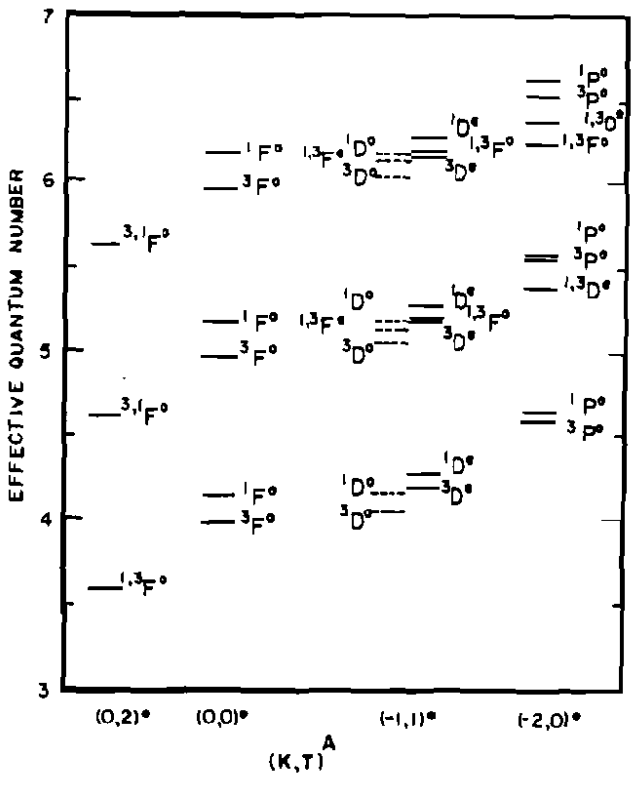

FIG. 20. Effective quantum numbers n^* for the $A = 0$ states of helium doubly excited states converging to the $N = 3$ limit of He^+ grouped according to $(K,T)^0$. Notice that the triplet state is always below the singlet state for a given K, T, and π. Notation like $^{1,3}F$ indicates that the two states are nearly degenerate, but ^1F is slightly above ^3F. The two $^{3,1}F$ cases are likely due to numerical inaccuracy. Data from Lipsky *et al.* (1977).

The discussion up to now summarizes the classification scheme and the spectroscopic regularities revealed through the introduction of correlation quantum numbers. Channels that have identical designation of correlation quantum numbers exhibit isomorphic correlation patterns and near-degenerate potential curves. This isomorphism is the underlying reason for the origin of the rotorlike supermultiplet structure of doubly excited states that have radial correlation quantum number $A = +1$ or -1. The discussion so far has been very descriptive for the purpose of presenting the classification scheme itself and for a general qualitative understanding of the correlation of doubly excited states. The rest of the article will provide an in-depth quantitative analysis on correlations in hyperspherical coordinates.

IV. Solution of the Two-Electron Schrödinger Equation in Hyperspherical Coordinates

In the previous two sections we discussed the results of the Schrödinger equation for two-electron atoms in the quasiseparable approximation for the classification of doubly excited states. In this section, we describe the computational methods used for the solution of the eigenvalue equation [Eq. (6)] and present some typical results.

A. Hyperspherical Harmonics and Solutions at Small R

We first examine the solution of Eq. (6) in the small-R limit. At small R, the kinetic energy term in Eq. (6) is proportional to $1/R^2$ while the Coulomb potential energy is proportional to $1/R$. In the limit of $R = 0$, Eq. (6) becomes

$$\left(-\frac{d^2}{d\alpha^2} + \frac{l_1^2}{\cos^2\alpha} + \frac{l_2^2}{\sin^2\alpha} - (\nu+2)^2\right) u_{l_1 l_2 m}(\Omega) = 0 \tag{20}$$

where $\nu = l_1 + l_2 + 2m$ and the eigenfunction $u_{l_1 l_2 m}$ is

$$u_{l_1 l_2 m} = f_{l_1 l_2 m}(\alpha)\mathcal{Y}_{l_1 l_2 LM}(\hat{r}_1, \hat{r}_2) \tag{21}$$

In Eq. (21), $\mathcal{Y}_{l_1 l_2 LM}(\hat{r}_1, \hat{r}_2)$ is the coupled angular momentum function of the two electrons,

$$\mathcal{Y}_{l_1 l_2 LM}(\hat{r}_1, \hat{r}_2) = \sum_{m_1 m_2} \langle l_1 m_1 l_2 m_2 | LM \rangle Y_{l_1 m_1}(\hat{r}_1) Y_{l_2 m_2}(\hat{r}_2) \tag{22}$$

and

$$f_{l_1 l_2 m}(\alpha) = N(\cos\alpha)^{l_1+1}(\sin\alpha)^{l_2+1} F(-m, m + l_1 + l_2 + 2 | l_2 + \tfrac{3}{2} | \sin^2\alpha) \tag{23}$$

where N is a normalization constant and F is proportional to a Jacobi polynomial (Morse and Feshbach, 1953). A properly (anti)symmetrized hyperspherical harmonic with respect to the interchange of two electrons is given by

$$\begin{aligned} U^{SLM}_{l_1 l_2 m}(\Omega) &= \frac{1}{\sqrt{2}}[f_{l_1 l_2 LM}(\alpha)\mathcal{Y}_{l_1 l_2 LM}(\hat{r}_1, \hat{r}_2) + (-1)^{l_1+l_2-L+S+m} f_{l_2 l_1 m}(\alpha) \\ &\quad \times \mathcal{Y}_{l_2 l_1 LM}(\hat{r}_1, \hat{r}_2)], \qquad \text{if} \quad l_1 \neq l_2 \\ &= \tfrac{1}{2}[1 + (-1)^{-L+S+m}] f_{llm}(\alpha)\mathcal{Y}_{llLM}(\hat{r}_1, \hat{r}_2), \qquad \text{if} \quad l_1 = l_2 = l \end{aligned} \tag{24}$$

In Eq. (24), the allowed values of m are such that $L + S + m =$ even if $l_1 = l_2$. Furthermore, the eigenvalue depends only on the sum, $\nu = l_1 + l_2 + 2m$.

In the $R \to 0$ limit, the quantum numbers l_1 and l_2 measure the barrier for the penetration of each individual electron into the inner region, while the quantum number ν measures the degree of simultaneous penetration of the two electrons into the small-R region. In this limit, the higher eigenvalues ν have a high degree of degeneracy. An analysis of $\nu = l_1 + l_2 + 2m$ alone can provide some indications about the nature of angular correlations that are missed in the independent-particle approximation. Strong correlation occurs when two or more eigenfunctions u with the same LS quantum numbers are degenerate. For example, this degeneracy occurs normally at $R = 0$ for $^1D^e$ channels with $(l_1, l_2) = (0,2)$ and with $(l_1, l_2) = (1,1)$ because they have the same $l_1 + l_2$. This degeneracy occurs for all even values of m so that the coupling between sd and pp states remains strong. This explains the strong interchannel coupling between the $ksnd\,^1D^e$ and $kp^2\,^1D^e$ states ($k < n$) of alkaline earth atoms along the whole $^1D^e$ series (O'Mahaony and Watanabe, 1985; O'Mahony, 1986; Lin, 1974b). Such mixing also explains the strong configuration mixing between $2snp^2\,^2D^e$ and $2s^2nd\,^2D^e$ in aluminum (Lin, 1974a; O'Mahony, 1986; Weiss, 1974). Similar analysis for the degeneracy of N-electron systems has been carried out recently by Cavagnero (1984).

B. The Asymptotic Limit and the Long-Range Dipole Approximation

In the asymptotic limit when one electron is inside and the other is far outside, corresponding to the limit that $R \to \infty$ and $\alpha \to 0$, the two-electron wave function is represented by the product of two independent-electron functions. In this limit, Eq. (6) can be easily solved by transforming R and α back to the independent-particle coordinates $r_2 = R \sin \alpha$ and $r_1 = R \cos \alpha = R$. If we expand the transformed equation in powers of $1/R$, the resulting asymptotic potential (Macek, 1968; Lin, 1974b) is

$$[U_\mu(R) - 1/4R^2 - W_{\mu\mu}(R)] \to -\frac{Z^2}{n^2} - \frac{2(Z-1)}{R} + \frac{1}{R^2}(\Phi_\mu|\mathbf{l}_1^2 + 2r_2 \cos\theta_{12}|\Phi_\mu) \quad (25)$$

If a_μ is the expectation value of $\mathbf{l}_1^2 + 2r_2 \cos\theta_{12}$ for channel μ, then the channel potentials within a given N manifold are distinguished by the different dipole terms a_μ/R^2. Such dipole potentials were first derived by Percival and Seaton (1957) and by Gailitis and Damburg (1963) from the close-coupling approximation in e–H^* scattering. It is called the dipole representation.

In previous works on dipole representation, each channel is labeled by the eigenvalues of Eq. (25). This method does not provide convenient integer quantum numbers. In order to be able to label the channels in the asymptotic limit, a "zero-order dipole basis" was proposed by Herrick (1975). In this approximate representation, only the dipole term $r_2 \cos\theta_{12}$ is diagonalized. Each channel for a given (N,L) is characterized by two quantum numbers, K and T. The eigenvalue of $r_2 \cos\theta_{12}$ in this representation $|NKTL\rangle$ is

$$\langle NKTL|r_2 \cos\theta_{12}|NKTL\rangle = -3NK/Z \quad (26)$$

Notice that this zero-order dipole operator is degenerate with respect to T. This degeneracy is removed if the centrifugal potential l_1^2 is included. In a perturbative calculation, Herrick (1975) showed that the dipole potential in the asymptotic limit is given by α_d/R^2, with

$$\alpha_d = -3NK/Z + L(L+1) + \tfrac{1}{2}(N^2 - 1 - K^2 - 3T^2) - (KZ/12N)[8L(L+1) + N^2 - 1 - K^2 - 15T^2] + \cdots \quad (27)$$

in the $|NKTL\rangle$ basis space.

Equation (27) provides the basis for labeling the potential curves in the asymptotic region, as discussed in Section III,B. According to Eq. (27), the effective dipole potential is most attractive for large positive K and, for a given K, a large value of T. Each $|NKTL\rangle$ channel basis is given as the linear combination of the product of hydrogenic Nl states and the spherical harmonics of the outer electron coupled to a total L. This channel function contains information about angular correlations but not radial correlations.

The asymptotic dipole potential for a given N, K, and T does not depend on the spin, nor on the parity of the channel. The fact that it does not depend on the parity of the channel is surprising since the l_1 and l_2 pairs which form the same L but different parity are quite different. This degeneracy is not the result of the perturbation calculation of Eq. (27). It can be shown that this degeneracy is exact from numerical calculations. Nikitin and Ostrovsky (1976, 1978) have derived the same conclusion from the group-symmetry viewpoint. The fact that the eigenvalues of Eq. (27) are independent of parity is important for discussing the T doubling in Section V,F.

C. Numerical Solution of the Channel Equations

The partial differential equation Eq. (6), can be solved by using an expansion

$$\Phi_\mu(R;\Omega) = A \sum_{[l_1 l_2]} g^\mu_{l_1 l_2}(R;\alpha)\mathcal{Y}_{l_1 l_2 LM}(\hat{r}_1, \hat{r}_2) \quad (28)$$

where A is the proper symmetrization or antisymmetrization operator (the spin function is not explicitly considered) and $\mathcal{Y}_{l_1 l_2 LM}(\hat{r}_1,\hat{r}_2)$ is the coupled angular momentum function defined in Eq. (22). We use the convention that $l_1 < l_2$ in the summation in Eq. (28).

With the substitution of Eq. (28) into Eq. (6), a set of coupled differential equations in the angle α are obtained. The number of equations is equal to the number of $[l_1,l_2]$ pairs included in Eq. (28). The resulting eigenvalue equations have been solved by different methods: (1) numerical integration of the coupled equations (Macek, 1968); (2) diagonalization using hyperspherical harmonics (Lin, 1974b; Klar and Klar, 1978, 1980); and (3) the finite difference method (Lin, 1975a, 1975b, 1976). All these methods have some limitations. The numerical integration method often suffers from instability and the finite difference method requires the solution of a large matrix if the number of $[l_1,l_2]$ pair is large. The diagonalization method is inaccurate at large R. At large R, the solutions are linear combinations of hydrogenic functions which cannot be expanded in terms of a small set of hyperspherical harmonics.

The calculation of the channel functions and the corresponding eigenvalues $U(R)$ is significantly simplified with the introduction of an analytical channel function for a given $[l_1,l_2]$ pair (Lin, 1981). The idea behind this is quite simple. It is best illustrated in terms of a few examples. Consider the lowest $^1S^e$ channel in the $[l_1,l_2] = [0,0]$ subspace. In the large-R limit,

$$g_{00}^{(1)}(R;\alpha) \xrightarrow[R\to\infty;\alpha\to 0]{} r_2 e^{-r_1} = R\sin\alpha e^{-R\sin\alpha} \tag{29}$$

to within a normalization constant. There are many different ways to generalize Eq. (29) to the small-R region. To do so, we require that the generalized functions reduce to the hyperspherical harmonics in the limit of $R = 0$. For the channel considered, this is proportional to $\sin 2\alpha$. A reasonable generalized function for this channel is then

$$g_{00}^{(1)}(R;\alpha) = N(R)\sin 2\alpha e^{-R\sin\alpha\cos\alpha} \tag{30}$$

This form reduces correctly to the known solutions in the $R = 0$ and $R \to \infty$ limits. The normalization $N(R)$ satisfies

$$\int_0^{\pi/2} [g_{00}^{(1)}(R;\alpha)]^2\, d\alpha = 1 \tag{31}$$

For the lowest $^3S^e$ channel in the [0,0] subspace, the generalized function is

$$g_{00}^{(1)}(R;\alpha) = N(R)\sin 2\alpha\cos 2\alpha e^{-R\sin\alpha\cos\alpha} \tag{32}$$

Notice that both Eqs. (30) and (32) satisfy the proper particle exchange symmetry under $\alpha \to \pi/2 - \alpha$ for ^1S and for ^3S, respectively.

This procedure can be extended to obtain analytical channel functions for other L, S, and π states and excited channels. The description for the construction of these functions was discussed by Lin (1981). With these analytical basis functions the calculation of channel functions $\Phi_\mu(R;\Omega)$ becomes very easy. In a typical calculation we include analytical channel functions and hyperspherical harmonics as basis functions to diagonalize the coupled differential equations. For example, to calculate all the potential curves for ^1S that lie below the $H(N = 3)$ or $He^+(N = 3)$ limits, a maximum of about fifteen basis functions including $[l_1,l_2] = [0,0]$, $[1,1]$, . . . , up to $[3,3]$ or $[4,4]$ is needed. The simplicity of the computational procedure allows us to study the properties of doubly excited states easily.

Other numerical methods have been proposed recently; see Christensen–Dalsgaard (1984a).

D. Representative Results for H^-

In this article, we are concerned mostly with the correlations of doubly excited states and the classification scheme. To show that the hyperspherical approach also gives reasonable quantitative results, we present in this section some representative results of H^- calculated using hyperspherical coordinates.

Consider the $^1P^0$ resonance states of H^- near the $H(N = 2)$ limit. The three potential curves that converge to this limit are shown in Fig. 21. Notice that

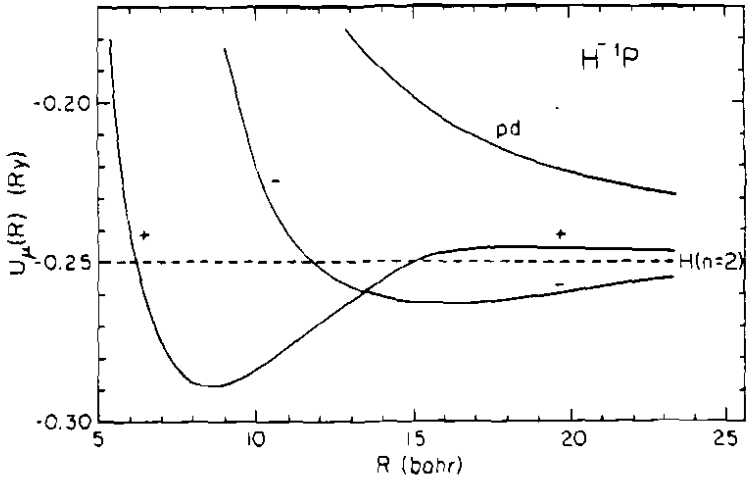

FIG. 21. Potential curves for the three $^1P^0$ channels of H^- that converge to the $N = 2$ limit of hydrogen. The +, −, and *pd* notations refer to the $(0,1)^+_{\frac{1}{2}}$, $(1,0)^-_{\frac{1}{2}}$, and $(-1,0)^+_{\frac{1}{2}}$ channels, respectively.

the $(0,1)^+$ channel has a relatively deep attractive potential well at small R, $R \approx 8$ a.u., but becomes repulsive at large R with a $2/R^2$ dependence (Lin, 1975b). The $(1,0)^-$ curve is quite repulsive at small R but has a very shallow attractive potential well at large R. The $(-1,0)^0$ curve is completely repulsive.

This example highlights the many aspects of correlation behaviors discussed in Sections III. The + channel has a more attractive potential at small R because of the in-phase radial correlation of the two electrons. It becomes repulsive at large R because for $K = 0$ the two electrons tend to stay near 90° from each other. The $(1,0)^-$ channel potential is not very attractive at small R because of its − character. It has a shallow potential well at large R, behaving asymptotically as $-3.71/R^2$ (Lin, 1975b), because of the favorable angular correlation that the two electrons maintain an angle close to 180° ($K = 1$). The $(-1,0)^\circ$ channel is completely repulsive owing to its unfavorable radial and angular correlations. In this channel, the two electrons are on the same side of the nucleus ($K < 0$), and they stay primarily in the valley region of the potential surface (Fig. 3).

The potential curves shown in Fig. 21 clearly suggest that resonances associated with the $(1,0)^-$ channel and those with the $(0,1)^+$ channel are quite different. The − channel is very repulsive at small R and thus the radial wave function (in R) is quite diffuse. By solving the hyperradial equation [Eq. (9)] using the − potential, the energy of the lowest state was found to be at −0.25191 Ry. Neglecting the small Lamb shift between the hydrogenic $2s$ and $2p$ states, this channel in principle can support an infinite number of states (Lin, 1976). But all the higher states are very close to the H($N = 2$) threshold and have not been observed experimentally. For the $(0,1)^+$ channel, the potential curve suggests the existence of shape resonances. In actual calculations, the + potential was found to support a shape resonance which is 32 meV above the threshold and has a width of 28 meV. Experimentally these resonances can be observed in electron–hydrogen atom scattering, but better data were obtained from the photodetachment of H^-. Because of the lack of suitable intense photon sources in the 10–15 eV region, such measurements were not done until recently. By taking advantage of the existence of the 800 MeV ($v/c = 0.83$) relativistic H^- beam from the LAMPF facility at Los Almos, Bryant *et al.* (1977) achieved the desired photon energy range by aiming lasers toward the incoming H^- beam at different angles. The lasers were blue-shifted to the desired photon energy range in the H^- frame.

The results of Bryant *et al.* (1977) for the photodetachment cross sections near the H($N = 2$) limit are shown in Fig. 22. It is clearly seen that the Feshbach resonance associated with the $(1,0)^-$ channel is quite narrow, and the shape resonance associated with the $(0,1)^+$ channel is much broader. The shape resonance was found to have a width of 23 ± 6 meV, and the separation of the Feshbach and shape resonances was found to be 53 meV. From the simple calculation using the quasi-separable approximation in hyperspherical coordinates, the corresponding results were 28 and 58 meV, respectively. More accurate calculations on these resonances have been performed by other methods. The solid line shown in Fig. 22 was due to Broad and Reinhardt (1976).

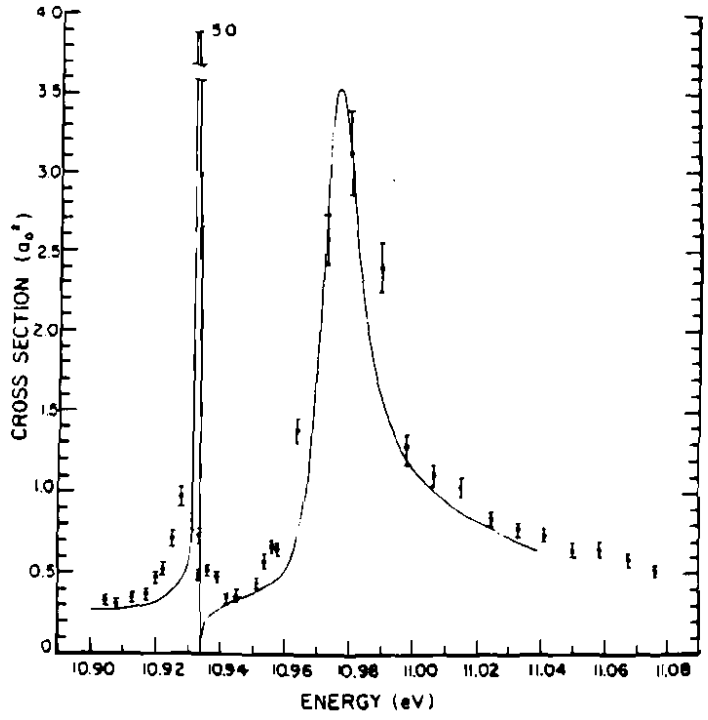

FIG. 22. Photodetachment cross sections of H^- near the $N = 2$ excitation threshold of hydrogen. The solid line is the result of the theoretical calculation of Broad and Reinhardt (1976) (Bryant *et al.*, 1977).

V. Body-Frame Analysis of Correlation Quantum Numbers

In Section III we presented a classification scheme of doubly excited states using the correlation quantum numbers K, T, and A. The angular correlation quantum numbers K and T, as discussed in Section IV, were adopted from

Herrick's work for the approximate description of Stark states in the asymptotic limits.

The adoption of quantum numbers in the asymptotic region for the description of doubly excited states seems unsatisfactory since important correlations occur in the region where the two electrons are close to each other. From Fig. 3, we notice that the potential surface is quite smooth along the θ_{12} coordinate. This smooth dependence allows us to expect that angular correlations do not vary significantly as R changes adiabatically. Similar conclusions have been obtained through actual numerical calculations (Lin, 1982b). We thus expect that the same quantum numbers K and T used in the asymptotic limit can be used to describe angular correlations in the inner region and also of the whole atom. To incorporate radial correlations, the quantum number A was introduced semiempirically (Lin, 1983d, 1984). In this section we re-examine these quantum numbers by analyzing the channel functions in the body frame of the atom (Watanabe and Lin, 1986).

A. Choice of the Body-Frame Axes

We choose the interelectronic axis

$$\hat{r}_{12} = (\mathbf{r}_1 - \mathbf{r}_2)/|\mathbf{r}_1 - \mathbf{r}_2| \tag{33}$$

as the internal axis of rotation. This choice is democratic with respect to the exchange of the two electrons. The general behavior of this axis is similar to that of the vector $\mathbf{B} = \mathbf{b}_1 - \mathbf{b}_2$ (Herrick and Sinanoglu, 1975a,b) exploited in the O(4) theory of doubly excited states since for a pure Coulomb field the Lenz vector $\mathbf{b}$ is related to $\mathbf{r}$ as

$$\mathbf{r} \to (3n/2Z)\mathbf{b} \tag{34}$$

where Z is the charge and n is the principal quantum number. For intrashell states the $\mathbf{B}$ in the O(4) theory is proportional to the interelectronic axis in Eq. (33). The choice of Eq. (33) as the internal axis also has the advantage of not specifying the principal quantum numbers n and N of the two electrons.

B. Decomposition into Rotational Components

In displaying the correlation patterns shown in Section III, the charge densities were averaged over the rotational angles of the whole atom. In this section, we decompose the whole wave function or channel function into components along the body-frame axis. Starting with a chosen laboratory frame, the rotation from the laboratory frame to the body frame is effected

through a rotation matrix

$$\mathcal{Y}_{l_1 l_2 LM}(\hat{r}_1, \hat{r}_2) = \sum_Q \mathcal{Y}_{l_1 l_2 LQ}(\hat{r}'_1, \hat{r}'_2) D^{(L)}_{QM}(\hat{\omega}) \tag{35}$$

where $(\hat{r}_1, \hat{r}_2)$ are defined in the laboratory frame and $(\hat{r}'_1, \hat{r}'_2)$ in the body frame, and D is a rotation matrix.

Suppose that the wave function is known in the laboratory coordinates,

$$\Psi(\mathbf{r}_1, \mathbf{r}_2) = \sum_{l_1 l_2} \Psi^L_{l_1 l_2}(r_1, r_2) \mathcal{Y}_{l_1 l_2 LM}(\hat{r}_1, \hat{r}_2) \tag{36}$$

Substitution of Eq. (35) into Eq. (36) gives

$$\Psi(\mathbf{r}_1, \mathbf{r}_2) = \sum_Q \psi^L_Q(R, \alpha, \theta_{12}) D^{(L)}_{QM}(\hat{\omega}) \tag{37}$$

where

$$\psi^L_Q(R, \alpha, \theta_{12}) = \sum_{l_1 l_2} \psi^L_{l_1 l_2}(R \cos\alpha, R \sin\alpha) \mathcal{Y}_{l_1 l_2 LQ}(\hat{r}'_1, \hat{r}'_2) \tag{38}$$

and $-L \leq Q \leq L$.

Let us consider the symmetry under particle exchange. A careful analysis in the Appendix of Watanabe and Lin (1986) shows that under $\alpha \to \pi/2 - \alpha$, each rotational component satisfies the property

$$\psi^L_Q(R, \pi/2 - \alpha, \theta_{12}) = \pi(-1)^{S+Q} \psi^L_Q(R, \alpha, \theta_{12}) \tag{39}$$

By introducing a phase factor A as

$$A = \pi(-1)^{S+T} \tag{40}$$

where $T = |Q|$, the index A determines the reflection symmetry of the radial wave function with respect to the $\alpha = \pi/4$ axis. Thus A serves as an index for radial correlations. In the special case $L = 0$, we have $T = 0$, $A = (-1)^S$, which is the well-known symmetry requirement for ^1S and ^3S states. For L not identical to zero, there are more than one rotational components. If there is only one dominant rotational component in Eq. (37), then the radial correlation quantum number A is determined from Eq. (40). In fact, Eq. (40) is identical to Eq. (18) for $A = +1$ or -1. We assigned $A = 0$ for those channels which do not have a major rotational component, even though each rotational component has its own well-defined symmetry in α.

Each rotational component also has a well-defined symmetry with respect to the $\theta_{12} = \pi$ axis. In fact, it can be shown that (Watanabe and Lin, 1986)

$$\psi^L_Q(R; \alpha, 2\pi - \theta_{12}) = (-1)^T \psi^L_Q(R; \alpha, \theta_{12}) \tag{41}$$

which provides the relation between the motion in θ_{12} and the rotational quantum number T.

C. Purity of Rotational States

The symbol A, as given by Eq. (40), has a close connection with the value of T. According to the decomposition of Eq. (37), if there is only one rotational component, then the radial correlation quantum number A will be either $A = +1$ or $A = -1$. Thus the purity of +/− radial correlation is related to the purity of rotational states.

To enrich our picture of the purity of rotational states, we show in Fig. 23 the decomposition of the $(1,1)_3^- {}^3P^0$ and $(1,1)_3^+ {}^1P^0$ channel functions at the values of R where their respective potentials bottom out. The percentage represents the contribution to the normalization from each T component. For $^3P^0$, the $T = 1$ component has 91% of the integrated density. According to Eqs. (40) and (41), for this component $A = -1$ and the function vanishes along $\theta_{12} = \pi$. The density plot for the $T = 1$ component clearly exhibits these properties. Figure 23 also shows that there is a 9% contribution of the $T = 0$ component for $^3P^0$ at $R = 23$. This component has $A = +1$ and an antinodal structure at $\theta_{12} = \pi$; the density plot for $T = 0$ clearly shows this behavior. Similarly, for $^1P^0$, the $T = 1$ component represents a 90% contribution and the $T = 0$ a 10% contribution at $R = 16$. In this case, the $T = 1$ component has $A = +1$ and a nodal structure at $\theta_{12} = \pi$, while the $T = 0$ component has $A = -1$ and an antinodal structure at $\theta_{12} = \pi$. The surface plot for each component exhibits these relations.

The purity of rotational states maximizes roughly in the range where the potential is near the minimum. To illustrate the dependence of the purity of

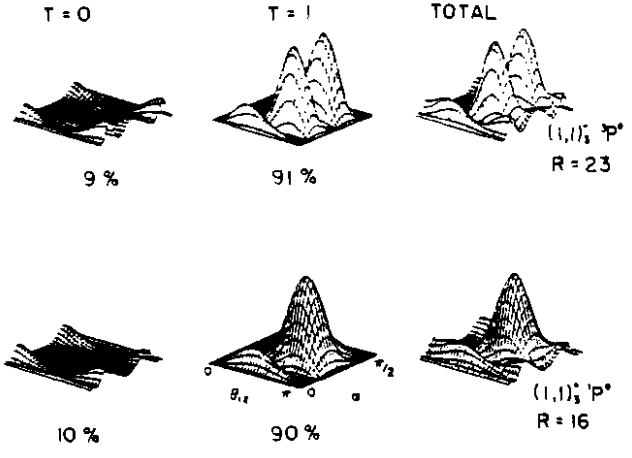

Fig. 23. Decomposition of the density plots into rotational components of the $(1,1)_3^- {}^3P^0$ and $(1,1)_3^+ {}^1P^0$ channels of He at the values of R indicated. The percentages represent the contribution to the normalization from each T component.

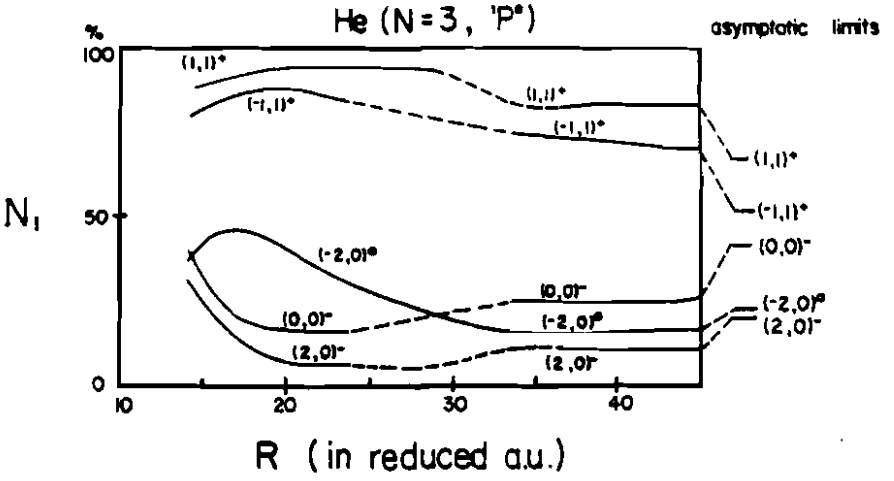

Fig. 24. Normalization coefficients for the $T = 1$ component for all five $^1P^0$ channels of helium below the $He^+(N = 3)$ limit. The asymptotic limits of the coefficients corresponding to $R \to \infty$ for each channel are indicated on the right. Dashed lines are used to indicate the region where diabatic crossing has been imposed.

rotational states on R for each channel, we show in Fig. 24 the normalization percentage of the $T = 1$ component for all of the five $^1P^0$ channels that converge to the $He^+(N = 3)$ thresholds. The dashed lines represent the interpolated region where the potential curves exhibit crossings. We note that the low-lying channels show greater purity of rotational states, while the higher channels violate the purity of T more severely. We further note that the rotational quantum number T is ill respected in the asymptotic region. The reason is that the angular motion of the outer electron is represented by the term l_1^2/R^2, which is not diagonal in the pure (K,T) basis.

D. Vibrational Quantum Numbers

Zero-order vibrational states do not emerge automatically from the body-frame analysis. To understand the quantum number K, we first assume every channel to be in a pure T state. Suppose that the outer electron approaches the inner one from a large distance. Take the axis of the approaching electron r_1 to be the z axis of the laboratory frame. In this frame, the two-electron angular momentum function is proportional to $P_Q^{l_2}(\cos\theta_{12})$, where $Q = \mathbf{L} \cdot \hat{r}_1$. The number of nodes in θ_{12} $(0 < \theta_{12} < \pi)$ is $l_2 - |Q|$, which varies between 0 and $N - 1 - T$. The transformation from the laboratory frame to the body frame is identity at large r_1; the transformation evolves smoothly to the small-R limit. Thus, for a given T, we can use the number of

nodes n in θ_{12} as a label for the vibrational motion in θ_{12}. In molecular physics, the vibrational quantum number v is related to n by

$$v = 2n + T \tag{42}$$

The quantum number K used for labeling hyperspherical channels is related to n and v by

$$K = N - 2n - T - 1 = N - v - 1 \tag{43}$$

When T is fixed, both v and K change in steps of 2.

The quantum numbers K and v have thus far been used as labels. According to the definition of K and T from the asymptotic solution, if a channel is a pure (K,T) state, the expectation value of the dipole moment $r_2 \cos\theta_{12}$ is $-(3N/2Z)K$. We can define a similar leading term in the dipole approximation which contributes to the vibrational energy

$$V_1(R;\alpha,\theta_{12}) = \frac{1}{R^2}\frac{R\sin\alpha}{\cos^2\alpha}\cos\theta_{12}, \qquad 0 \leq \alpha \leq \pi/4$$

$$= \frac{1}{R^2}\frac{R\cos\alpha}{\sin^2\alpha}\cos\theta_{12}, \qquad \pi/4 \leq \alpha \leq \pi/2 \tag{44}$$

Here R^2V_1 determines the polarizability of the system. To examine the purity of an effective $\bar{K}$, we define

$$\bar{K}(R) = -\left(\frac{2Z}{3N}\right)R^2\langle V_1\rangle \tag{45}$$

The results for $\bar{K}(R)$ for He($N = 3$, $^1P^0$) channels are shown in Fig. 25. We note that $\bar{K}(R)$ indeed varies slowly with R and is very close to the integers K used to label the channels, particularly for the low-lying channels.

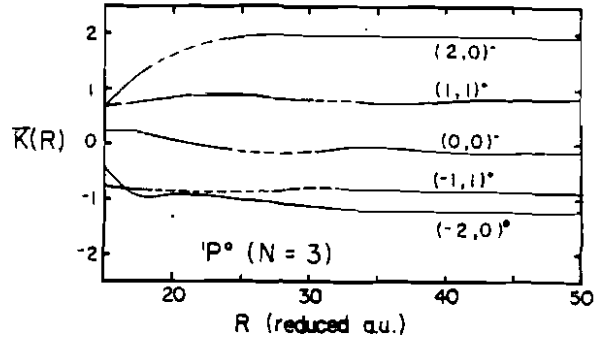

FIG. 25. R dependence of the $\bar{K}(R)$ defined by Eq. (45) for the $^1P^o(N = 3)$ manifold of He. Dashed lines are used to indicate the region where diabatic crossing has been imposed.

E. Moleculelike Viewpoint of Two-Electron Correlations

The body-frame analysis so far indicates that the quantum numbers K and T can be related to the vibrational and rotational quantum numbers used in molecular physics. This rovibrational viewpoint has been explored extensively for intrashell states (Herrick *et al.*, 1980; Kellman and Herrick, 1978, 1980; Herrick, 1983) and for model two-electron atoms (Ezra and Berry, 1982, 1983). By generalizing to intershell states, one can identify (Watanabe and Lin, 1986) the +/− radial quantum numbers as the symmetric stretch (for $A = +$) and antisymmetric stretch modes used by quantum chemists (see the review by Manz, 1985). The potential curves illustrated in Figs. 12–14 and the energy levels shown in Figs. 17 and 18 indicate that the magnitude of the correlation energies follow the hierarchical order

$$U_A > U_K > U_T \tag{46}$$

where U_A, U_K, U_T are the separation of the $A = +$ and $-$ doublet curves and the local vibrational and rotational energies, respectively. The higher excitations, particularly the $A = 0$ channels, lead to the less clear-cut order and to a noticeable admixture of other modes. These higher excitations do not exhibit moleculelike modes.

After the moleculelike modes have been divided into $A = +$ and $A = -$ groups, angular correlations can be classified by their degree of excitations. There are two well-defined schemes (Herrick, 1983) which can be easily understood from Eq. (46). One is the d-supermultiplet scheme which utilizes the number of nodes in θ_{12}, namely the n discussed in the previous subsection, to regroup angular correlation patterns. An example is shown in Fig. 26 for the lowest $n = 0$ states for the $A = +$ and for the $A = -$ subgroups for doubly excited states of He($N = 3$). The vertical axis corresponds to L and the horizontal axis is labeled by $\pm T$, where we have used $-T$ to designate states which have rotational quantum number T but with parity given by $\pi = (-1)^{L+1}$ in order to distinguish it from states with identical T but with parity $\pi = (-1)^L$. Note that there is a clear correspondence between the "+"-type and "−"-type supermultiplets, namely the interchange of the spin label $1 \leftrightarrow 3$. Another scheme is known as the I supermultiplets. Defining $I = L - T$, loosely speaking, I corresponds to the rotational degree of freedom orthogonal to that represented by T (Watanabe and Lin, 1986). With K as the vertical axis and $\pm T$ as the horizontal axis, a diamond similar to Fig. 26 can be constructed for each I (Herrick *et al.*, 1980).

The moleculelike normal modes motivated Kellman and Herrick (1980)

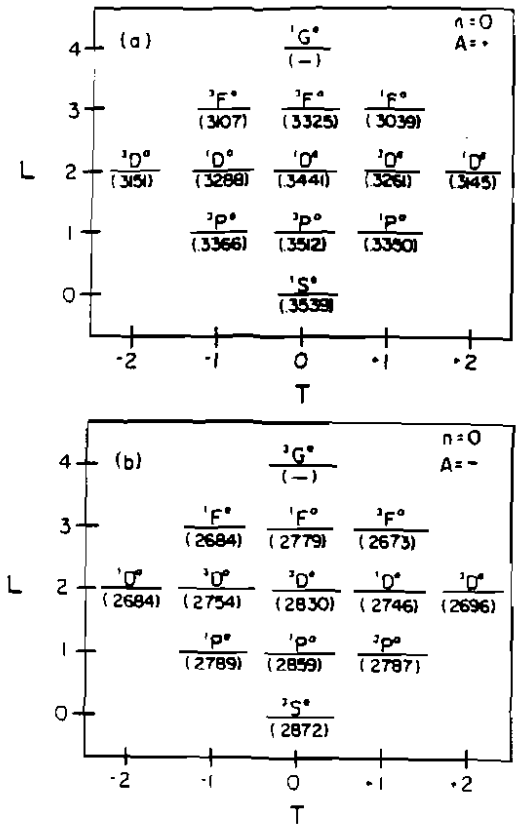

FIG. 26. d-Supermultiplet structure of helium doubly excited states below the $N = 3$ limit of He^+. (a) Intrashell states; (b) the lowest states of all the $A = -1$ channels. Energy levels from Lipsky *et al.* (1977).

to fit intrashell energy levels to the molecular term formula

$$E = E_N + \omega(V+1) + X(V+1)^2 + GT^2 + [B - \alpha(V+1)][L(L+1) - T^2] - D[L(L+1) - T^2] \quad (47)$$

This formula attempts to attribute all the higher-order corrections to the anharmonicity of the bending vibrational potential, centrifugal distortion, etc. In atoms, the impurity of the (K,T) states owing to angular excitation is an equally important contributor to the departure from the lowest-order formula

$$E = E_N + \omega(V+1) + B[L(L+1) - T^2] + GT^2 \quad (48)$$

A more detailed discussion on the limitation of the moleculelike interpretation of doubly excited states is given in Watanabe and Lin (1986).

F. The T Doubling

In Fig. 17 we note that each pair of $T \neq 0$ states which have identical n, N, A, L, and K have near-degenerate energies. The splitting of each pair is called T doubling. T doubling occurs for $A = +1$ as well as for $A = -1$ states. In fact, it also occurs for $A = 0$ states, as shown in Fig. 20 for states belonging to the $(-1,1)^0$ channel.

The effective principal quantum numbers shown in Figs. 17 and 20 clearly indicate that between each pair of states the energy of the state with parity $\pi = (-1)^{L+1}$ is slightly lower than that of the state with parity $\pi = (-1)^L$. This difference can be attributed to the wave functions near $\theta_{12} = 0$. It can be shown (Rehmus *et al.*, 1978; Ezra and Berry, 1982) that the wave functions for states with parity $\pi = (-1)^{L+1}$ vanish identically at $\theta_{12} = 0$. There is no such constraint for states with parity $\pi = (-1)^L$. In general, the wave functions for these latter states are small at $\theta_{12} = 0$ and $\alpha = \pi/4$, but they do not exactly vanish.

A nonzero amplitude near $\theta_{12} = 0$ and $\alpha = \pi/4$ tends to increase the electron–electron repulsion energy. If all the other quantum numbers, n, N, A, L, K, and T, are the same for the pair of states, such a stronger electron–electron repulsion would result in a higher energy for the state with parity $\pi = (-1)^L$. The energy levels in Fig. 17 are in agreement with this prediction [see the $(1,1)^+$, $(0,2)^+$, and $(-1,1)^+$ series in the upper frame and the $(1,1)^-$, $(0,2)^-$, and $(-1,1)^-$ series in the lower frame]. This prediction, however, is not completely confirmed by the results shown in Fig. 18 for the resonances of H^- below the $H(N = 5)$ threshold (Ho and Callaway, 1983). The calculated energy ordering for the $(2,2)^+$ and $(1,1)^+$ channels is opposite to what we have expected. Whether this irregularity in the T doubling is due to some other unaccounted effects or due to the inaccuracy in numerical calculations remains to be resolved. Similar irregularities in this respect can also be found in the calculated energies for the resonances of H^- below the $H(N = 4)$ threshold [see Table II of Ho and Callaway (1983)].

G. Systematics of Autoionization Widths

One of the most striking features of the earlier photoabsorption data of doubly excited states of helium is that the autoionization widths of different Rydberg series are dramatically different. To characterize the width of a

Rydberg series, we define a reduced width, $\bar{\Gamma} = n^{*3}\,\Gamma_n$, where Γ_n is the autoionization width of state n with effective principal quantum number n^*. (It is well known that the reduced width defined this way is nearly constant along the series.) From the data of Madden and Codling (1963, 1965), as well as the results of early close-coupling calculations (Burke and McVicar, 1965; Burke and Taylor, 1966; see also Fano, 1969), it was shown that the ratios for the reduced widths of the three $^1P^0$ series, $(0,1)^+_{\frac{1}{2}}$, $(1,0)^-_{\frac{1}{2}}$, and $(-1,0)^e_{\frac{1}{2}}$, are 3000: 30: 1. Such drastic differences in widths are typical when we compare $A = +1$, -1, and 0 channels.

The systematics of autoionization widths with respect to other quantum numbers are less clear, although fragmentary evidences and "rules of thumb" have been discussed (Herrick, 1983; Rehmus and Berry, 1981; Watanabe and Lin, 1986). These rules are "understood" in terms of the correlation properties or in terms of the moleculelike normal modes of doubly excited states.

(1) The partial width is largest when the continuum channel corresponds to $\Delta N = -1$, $\Delta K = -1$ (i.e., $\Delta v = 0$), $\Delta T = 0$, with A unchanged. This rule is easily understood because the overlap between this continuum channel and the quasi-bound resonance is largest owing to their similar correlation patterns. The overlap occurs mostly near the locus of the ridge (Fano, 1981) where the pair correlation in the continuum channel is just breaking up and the quasi-bound resonant wave function is gaining amplitude.

(2) The widths for the pair of T doublets are nearly identical. This is well supported by existing calculations (Ho and Callaway, 1983, 1984). Since the lower state of the T doublet has less amplitude near $\alpha = \pi/4$ and $\theta_{12} = 0$, it is expected that this state has smaller width. The results given by Ho and Callaway (1983) for the resonances of H^- converging to $N = 4$ and 5 of H thresholds do not support this prediction. It is not clear that this discrepancy is due to the neglect of other effects or because of numerical inaccuracies.

(3) Along a rotor series, states with higher L have larger widths. This is because the higher rotor states have larger amplitudes near $\theta_{12} = 0$. This effect can be overtaken by the fact that the higher rotor states have less amplitude near $\alpha = \pi/4$. For example, the $(4,0)^+_5$ rotor series of H^-, $^1S^e$, $^3P^0$, $^1D^e$, $^3F^0$, $^1G^e$, $^3H^0$, $^1I^e$, and $^3K^0$, as shown in Fig. 18, have widths, in units of 10^{-3} Ry, of 1.1, 1.2, 1.3, 1.2, 1.5, 1.8, 0.54, and 0.2 (Ho and Callaway, 1983).

(4) When n, N, L, S, π, and K are the same, the states with the larger T have the larger widths. This is due to the increase in the amplitude near $\theta_{12} = 0$ for higher T states. For example, the $(0,2)^+_5$ $^1D^e$ state of He is a factor of 3.5 broader than the state $(0,0)^+_5$ $^1D^e$ (Herrick and Sinanoglu, 1975a). There are very few other calculations to check the validity of this rule.

These rules were drawn from the few data currently available with "plausible" explanations provided from the correlation properties. Since the autoionization width depends sensitively on the details of the wave functions of the quasi-bound state and the continuum state, it is interesting to find out what systematics of autoionization widths can be drawn from the correlation properties of the quasi-bound-state wave function alone. Extensive compilation of widths in future calculations will help to check the generality of these rules.

VI. Effects of Strong Electric Fields on Resonance Structures in H^- Photodetachment

A. Experimental Results

In this section the effect of electric fields on the resonances of H^- is discussed. We will not address the large area of the Stark effect of Rydberg electrons; rather, we will concentrate on the effect of electric fields on the doubly excited states of H^-, where experimental data have been obtained by Bryant and coworkers at the LAMPF facility at Los Almos. In their experiments, an external magnetic field up to several kG is applied to the relativistic H^- beam (see Section IV,E) which corresponds to an electric field of up to a few MV/cm in the H^- frame. Their results are summarized as follows.

(1) The $^1P^0$ Feshbach resonance below the H($N = 2$) discussed in Section IV,E was found by Gram *et al.* (1978) to split into three components; the two outer components exhibit linear Stark shifts and the middle one exhibits quadratic Stark shift. Later experiments by the same group (Bryant *et al.*, 1983) with the use of polarized laser light confirmed that the two outer components belong to states which have a magnetic quantum number $M = 0$ and the middle one has $|M| = 1$. Their results are displayed here in Fig. 27. We notice that the lowest component was observed to quench at $E \sim 130$ kV/cm, the middle branch was found to vanish at around 270 kV/cm, while the upper branch appears to burrow into the shape resonance for fields higher than 400 kV/cm.

(2) The shape resonance was observed to be quite stable against the electric field. The results from Bryant *et al.* (1983) for the width of the shape resonance in the electric field are shown in Fig. 28. Initially the width decreases as the field is increased to about 0.2 MV/cm, then it increases rapidly with the field until 0.7 MV/cm, where its rate of increase begins to decline. There is no

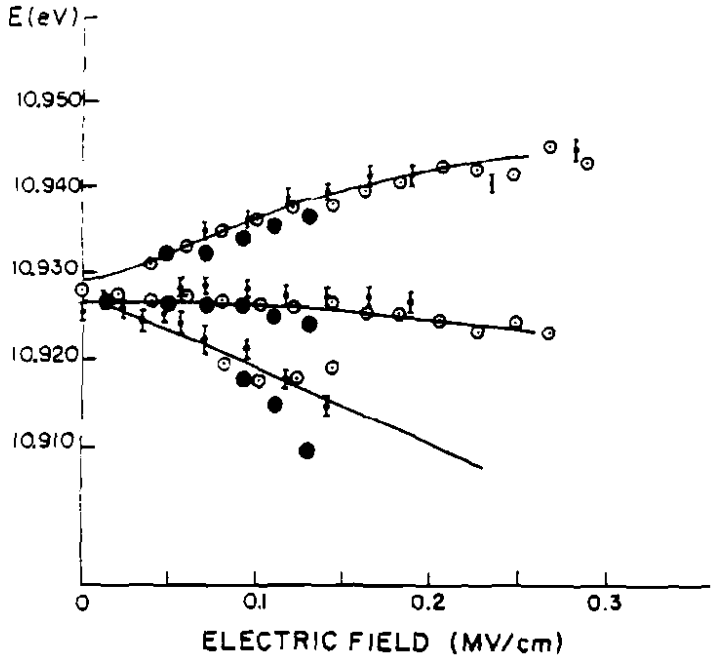

FIG. 27. Energies of the centroids of Feshbach multiplets as a function of applied electric field. Solid lines are from the theoretical results of Callaway and Rau (1978) (Bryant *et al.*, 1983); (⊙) "σ polarization," curved prism; (ǂ "π polarization," flat prism; (●) nitrogen laser, unpolarized.

experimental information about the field at which the shape resonance is quenched.

(3) The $^1D^e$ resonance which has a corresponding photon energy of 10.874 eV can be excited by single-photon transitions in an electric field. Indeed, a structure at approximately the expected energy of this resonance was observed for fields in excess of 400 kV/cm. It appears that this resonance splits into two at the higher field.

(4) The stripping of the ground state of H^- in a strong electric field has also been measured by Bryant's group (private communication, 1983). Their results, together with the earlier weak-field data from other groups, are displayed in Fig. 29.

These strong-field results are quite interesting in several respects. Since the resonances studied belong to different channels, the energy shift as well as the change of the width for each resonance is characterized by the correlated motions of the two electrons and their relation with respect to the direction of the electric field.

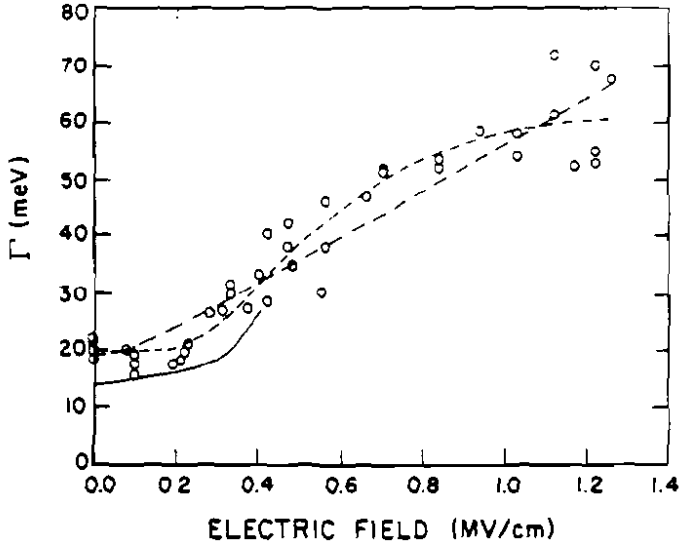

FIG. 28. Width of shape resonance versus applied electric field. (———) From the theory of Wendoloski and Reinhardt (1978). (— · —) and (– – –) are two different fits to the experimental data (Bryant *et al.*, 1983).

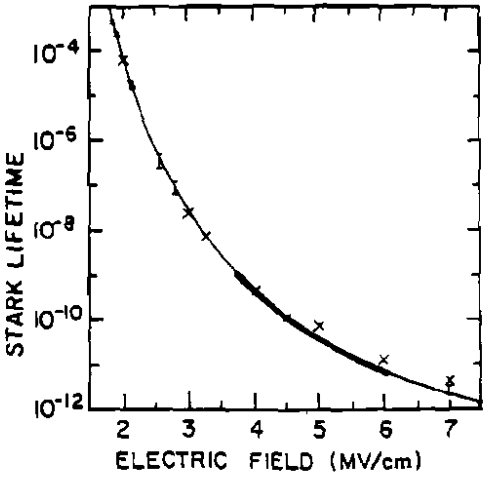

FIG. 29. Quenching lifetimes for the ground state of H^- in an electric field. The thick solid line is from the data of Bryant (1983, private communication). The crosses are the results calculated from the field-modified hyperspherical potential curves.

B. Theoretical Interpretations

A preliminary study on the effect of strong electric fields on the resonances of H^- has been initiated using the quasiseparable approximation in hyperspherical coordinates (Lin, 1983c). The basic method is similar to that which was described in Section II except that the potential due to the Stark field is included nonperturbatively in the new Hamiltonian. Using the analytical basis functions of Section IV, the effective potential curves for each given electric field can be obtained. These potential curves are used to interpret semiquantitatively the observations of Bryant *et al.* (1983).

(1) We first show that the lifetime of the ground state of H^- in an electric field can be understood using this simple picture. In Fig. 30 we show the adiabatic potential curves of the lowest channel of H^- in different electric fields in units of MV/cm. We notice that the effect of the electric field is to introduce a linearly decreasing potential in the large-R region, while the small-R region is hardly affected. In terms of this picture, the lifetime of the ground state of H^- can be estimated using the tunneling model similar to that used to describe the α-decay of nuclei. With potentials as shown in Fig. 30, the lifetime of the ground state can be estimated using a WKB approximation. The results of such an estimate are shown by the crosses in Fig. 29. They are in good agreement with the measured results from the low-field to the high-field region. The discrepancy at the higher fields is probably due to

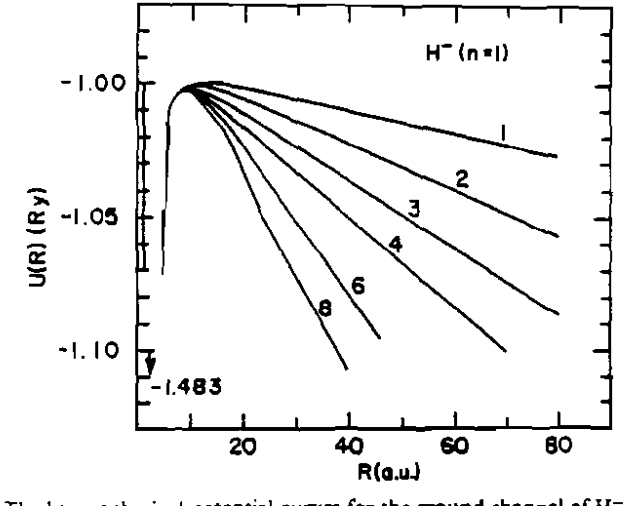

Fig. 30. The hyperspherical potential curves for the ground channel of H^- in an electric field.

the breakdown of the WKB approximation when the barrier penetration is large.

(2) The linear Stark shifts of the zero-field Feshbach resonances can be understood in terms of mixing with a nearly degenerate state with the same spin, but opposite parity: the second recursion of a $^1S^e$ Feshbach sequence converging to the $N = 2$ series limit. Such shifts can be calculated using the diagonalization of a large set of basis functions. The results of such a calculation by Callaway and Rau (1978) are shown as solid lines in Fig. 27. Such calculations, however, give only the shifts and provide no information about the quenching. Using the quasiseparable approximation in hyperspherical coordinates, the potential curves for the two $M = 0$ Stark states shown in Fig. 31 can be calculated. In Fig. 31a we see that the dependence of the potential curves with the electric field is similar to those shown in Fig. 30 for the ground channel. As the field increases, the potentials in the outer regions decrease linearly with R with little change in the inner region. From the dependence of the potentials with the E field, a simple estimate based upon first-order perturbation theory indicates that the energy shift depends lin-

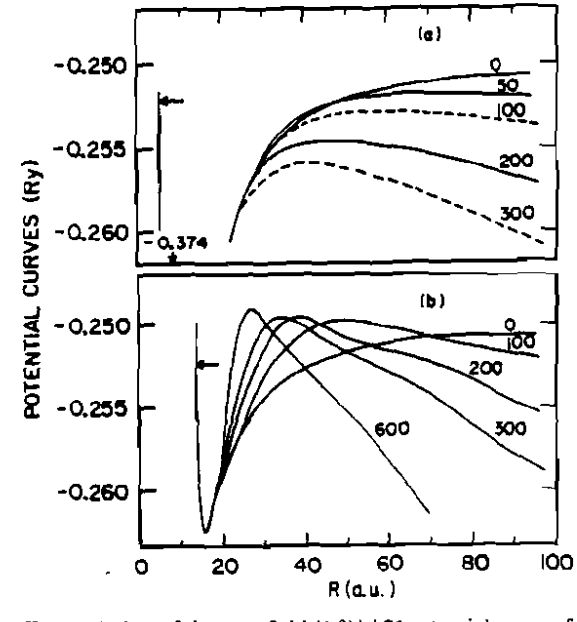

Fig. 31. (a) The variation of the zero-field $(1.0)^+_1$ $^1S^e$ potential curve of H^- in an electric field. The electric fields are given in units of kV/cm. (b) Same as (a) but for the zero-field $(1,0)^-_2$ $^1P^o$ channel of H^-. The two horizontal arrows indicate the position of field-free resonances.

early on the strength of the electric field. The classical field ionization occurs at $E \sim 100$ kV/cm, which is consistent with the experimental value of 140 kV/cm.

The upper linear Stark component exhibits a somewhat unfamiliar dependence on the electric field. As shown in Fig. 31b, when the electric field is applied the potential curve in the inner portion is shifted upward, while the outer portion of the curve is shifted downward with increasing electric field. In fact, in Fig. 31b we notice that the barrier height is above the field-free threshold at -0.25 Ry.

The behavior of the potential curves in Fig. 31b clearly indicates an upward Stark shift of its eigenvalue; a first-order perturbation calculation indicates that the shift is linear with E at small electric fields. The decay width of the resonance, because of the increase in the height of the barrier with the electric field, is expected to become narrower at lower fields before it broadens again at higher fields. A simple WKB estimate based on the calculated potential curves indicates that the inner potential is no longer attractive enough to support a bound state at $E \sim 350$ kV/cm. Experimental data do not give the field where this state is quenched since it lies in the shoulder of the broadened shape resonance.

(3) The effective potential curves in electric fields for the shape resonance behave similarly to those shown in Fig. 31b; in a weak field the potential barrier becomes higher while the potential at large R decreases linearly with R [see Fig. 3 of Lin (1983c)]. Such dependence implies that the width of the shape resonance becomes narrower in a weak electric field before it becomes broader as the field increases. The narrowing of the shape resonance was observed by Bryant *et al.* (1983), as shown in Fig. 28, but the data also indicate that the width increases rapidly for $E > 400$ kV/cm. This broadening cannot be explained by the calculated effective potentials.

The blue shifts of the spectral lines and the narrowing of the resonances in an electric field are not difficult to understand. In a given electric field, electrons in the lower channels tend to line up opposite to the direction of the electric field. In the higher channels, the orthogonality condition of the wave functions with respect to lower channels requires that the electrons occupy regions perpendicular to the field or toward the direction of the field. Such rearrangement of the charge cloud tends to increase the energy of the state as well as to render the state more stable against field quenching.

The simple interpretation presented here for the strong field effects on the resonances is not complete. In an electric field, a resonance state can be quenched. Its energy is shifted by the electric field in addition to the autoionization. A complete quantitative evaluation of all these effects requires a full treatment of the multichannel scattering aspect of the problem.

VII. Doubly Excited States of Multielectron Atoms

So far our discussions have been centered on the doubly excited states of two-electron atoms, He and H^-. In this section, we briefly describe the progress made in the understanding of doubly excited states of multielectron atoms.

A. Alkali Negative Ions and Alkaline Earth Atoms

For these two-valence-electron systems, the electron pair of interest is attracted to an ionic core which is spherically symmetric when both electrons are outside the core. Under this restriction, the electron pair experiences primarily an attractive Coulomb potential plus a weaker polarization potential. On the other hand, penetration of either electron within the core exposes that electron to a stronger field and to substantial exchange of energy and angular momentum with the core electrons. These effects are minimal for two-valence-electron systems where the core can be regarded as "frozen." Therefore, these systems are similar to two-electron systems.

For the two-valence-electron systems, the electron–core interaction is no longer Coulombic, and the single particle states in the asymptotic limits within the same N manifold are no longer degenerate. Thus K and T quantum numbers, as defined according to the analysis of Stark states, are no longer valid when such degeneracy is removed. On the other hand, our body-frame analysis of the correlation quantum numbers does not rely upon such degeneracy. The interesting question to be answered is whether the classification scheme and the properties of doubly excited states unraveled for the pure two-electron systems remain valid for doubly excited states of multielectron systems.

By approximating the electron–core interaction by a suitably chosen model potential, these two-valence-electron atoms can be solved in hyperspherical coordinates (Greene, 1981; Lin, 1983b). The two $^1S^e$ potential curves of Be which converge to the $2s$ and $2p$ states of Be^+ are shown in Fig. 32. They are labeled in terms of the independent-particle designations, $2s\epsilon s$ and $2p\epsilon p$. These notations are by no means adequate. In Fig. 33, the surface charge density plots for the two channels at different values of R are displayed. For $R = 2$ and 6, we notice that these plots are quite similar to the plots for the $(1,0)^+$ channel of H^- shown in Fig. 8. At large R, especially $R = 14$, the surface plot becomes similar to what one would have expected for the $2s\epsilon s\ ^1S^e$, where there is little angular correlation and the channel function shows little θ_{12} dependence. Similarly, for the "$2p\epsilon p$" channel, the

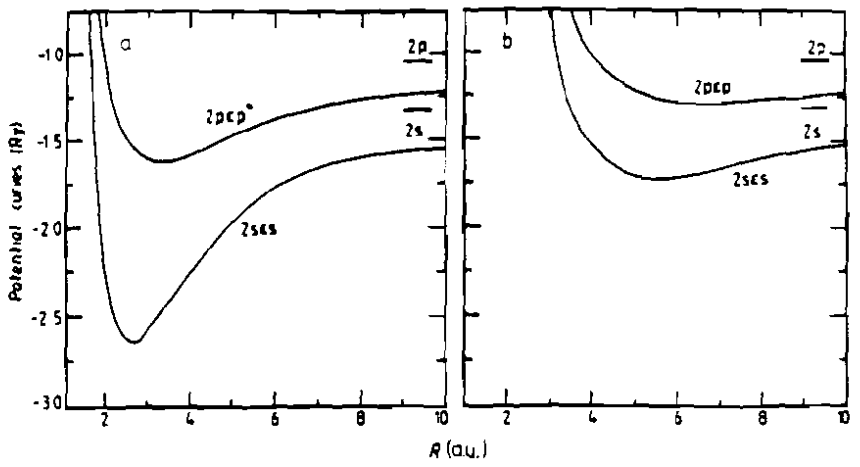

FIG. 32. Adiabatic potential curves of (a) Be $^1S^e$ and (b) Be $^3S^e$ channels converging to $2s$ and $2p$ states of Be^+. The channels are labeled using quantum numbers according to the independent-particle approximation.

charge distributions shown in Fig. 33b for small values of R resemble the $(-1,0)^+$ channel shown in Fig. 8. At large R, these plots are consistent with the designation $2p\epsilon p\ ^1S^e$, as the densities show a $\cos^2\theta_{12}$ dependence. These plots clearly indicate that the designations "$2s\epsilon s$" and "$2p\epsilon p$" are suitable for the large-R region and the $(1,0)^+$ and $(-1,0)^+$ notations are more suitable for the small-R region. In terms of the description of individual states, the single-particle designations $2snS$ and $2pnP$ are more appropriate for excited states ($n \gg 2$), and ${}_n(K,T)^A_N$ designations are more appropriate for intrashell states.

The adiabatic approximation was found to be valid for the two $^1S^e$ channels of Be shown, as the coupling between the two channels was found to be small. Despite the fact that the angular correlation does not remain constant for each channel as R changes (as in the pure two-electron case), the angular correlation does evolve smoothly with R. Energy levels calculated from each adiabatic potential were found to be in good agreement with experimental data and with other calculations (see Lin, 1983b).

It is interesting to ask if radial correlations are preserved for the two-valence-electron systems along the adiabatic channel. The adiabatic potential curves for the three $^1P^0$ and three $^3P^0$ channels of Be below the $2s$ and $2p$ states of Be^+ are shown in Fig. 34. They were labeled as $2snp$, $2pns$, and $2pnd$ (Lin, 1983b). By examining the $[l_1,l_2] = [0,1]$ component of the channel function, Greene (1981) has shown that the α-dependent part [$g(\alpha)$ of Eq. (13)] of the $2snp$ channel exhibits "+"-type behavior at small R, but it

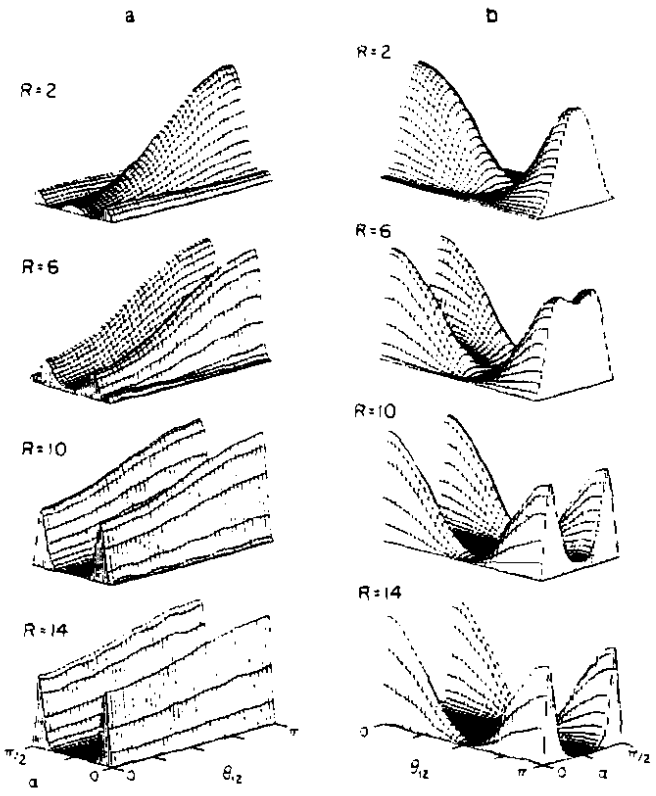

FIG. 33. Surface charge-density plots for (a) Be $2s\epsilon s\ ^1S^e$ and (b) Be $2p\epsilon p\ ^1S^e$ channels on the (α,θ_{12}) plane for different values of R. Notice that the graphs are oriented differently along the channels. The surface plots for the $2s\epsilon s$ channel at small R are similar to the plots for the $(1,0)^+_2$ channel, and those for the $2p\epsilon p\ ^1S^e$ at small R are similar to the plots for the $(-1,0)^+_2$ channel of two-electron atoms. (See Fig. 8.)

evolves into a function similar to the hydrogenic $2s$ at large R. The $2pns$ channel exhibits "$-$"-type behavior at small R and evolves into a function similar to a hydrogenic $2p$ function at large R. These results are shown in Fig. 35. These plots are to be compared with the two graphs shown in Fig. 6 for He.

In Fig. 34 we also note that the $2snp$ and $2pns$ curves have a pronounced avoided crossing at $R = 5$ a.u. It was found that the coupling term between the two adiabatic channels is relatively large. Unlike the +/− crossing for the $^1P^0$ (see Fig. 21) in H^-, this avoided crossing cannot be treated diabatically. It turns out that the physical states are better represented by a linear combination of the adiabatic channels. By solving the coupled radial equations,

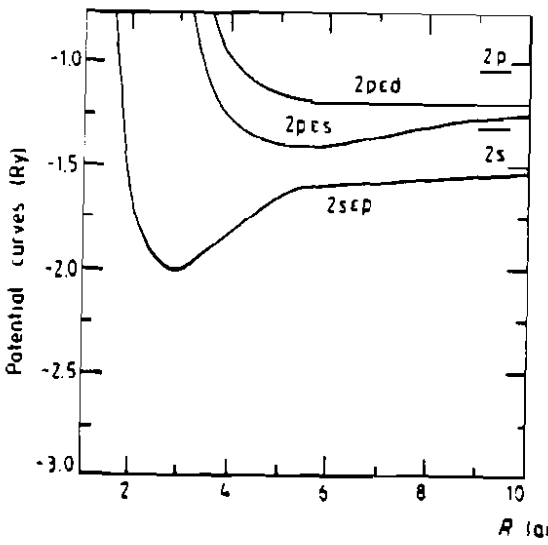

FIG. 34. Adiabatic potential curves of (a) Be $^1P^0$ and (b) Be $^3P^0$ channels converging to the $2s$ and $2p$ states of Be^+. Notice the strong avoided crossing between the $2s\varepsilon p$ and $2p\varepsilon s$ $^1P^0$ channels at $R \sim 5$ a.u.

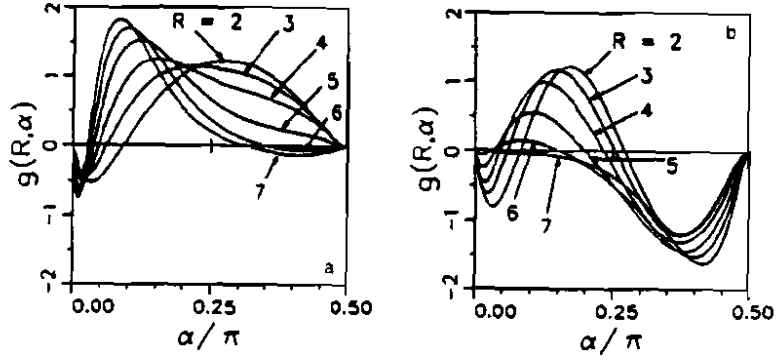

FIG. 35. Variations of the α-dependent part of the channel functions [see $g(\alpha)$ of Eq. (13)] at various values of R for the (a) $2s\varepsilon p$ and (b) $2p\varepsilon s$ $^1P^0$ channels of Be. For small values of R, $g(\alpha)$ shows behavior similar to the + radial correlations for the $2s\varepsilon p$ channel and − radial correlations for the $2p\varepsilon s$ channel (cf. Fig. 7). At large R, $g(\alpha)$ for the $2s\varepsilon p$ channel reduces to a $2s$-type radial wave function in the small-α region with vanishing amplitudes for $\alpha \sim \pi/2$. For the $2p\varepsilon s$ channel, $g(\alpha)$ is very small in the small-α region but it behaves like a $2p$ radial function for $\alpha \sim \pi/2$.

Greene (1981) has shown that the quantum defects for the $2snp$ and $2pns$ states are much improved over those obtained from a single adiabatic channel calculation.

Further work along this line has been shown recently by O'Mahony and Watanabe (1985) on the $^1D^e$ spectrum of Be. Their work departs from the pure hyperspherical procedure in that they use the R-matrix method to obtain reliable data, but hyperspherical wave functions were used to present a more transparent picture of electron correlations as well as to delineate the regions of space at which channel coupling occurs. O'Mahony (1986) also studied the Mg I $^1D^e$ spectrum and extended the method to analyze the channel interactions in the $^2D^e$ spectrum of Al I, thus casting the qualitative analysis of Section IV,A on a quantitative basis.

As we proceed to doubly excited states converging to the higher N manifold, the correlations and channel behaviors of the states become closer to those exhibited in the corresponding channels in H^- and in He. In Fig. 36 we show the potential curves of the three lowest $^1P^0$ and $^3P^0$ states of Li^- that lie below the $3s$, $3p$, and $3d$ levels of Li. Note that the curves show diabatic crossing similar to those shown in Fig. 12 for He. No systematic studies of the correlations of these systems have been accomplished yet. It would be interesting to examine how the supermultiplet structure of Section IV is modified for systems like beryllium.

Doubly excited states of other alkaline earths and alkali negative ions have

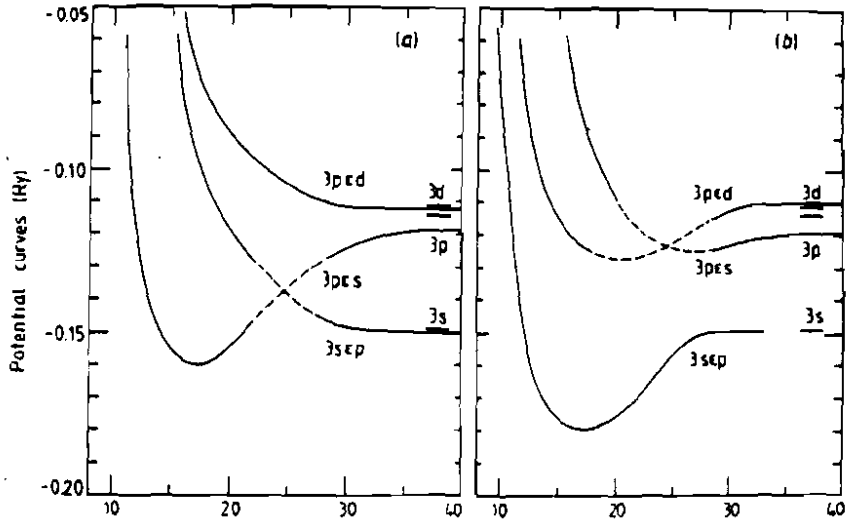

FIG. 36. Potential curves for (a) $^1P^0$ and (b) $^3P^0$ of Li^- converging to the $N = 3$ limits of Li.

also been studied by Greene (1981) and by Watanabe and Greene (1980). These subjects have been reviewed by Fano (1983).

B. Doubly Excited States of He^-

Doubly excited states of multielectron atoms in general consist of an electron pair outside a compact open-shell core. The core can be viewed as a perturber that scatters individually one of the outer electrons with a possible exchange of spin. For He^-, these doubly excited states appear as resonances in e–He scattering. An ever-increasing volume of experimental results for resonances associated with the $N = 2$ and 3 limits of He have been accumulated (Brunt *et al.*, 1977; Buckman *et al.*, 1983; Schultz, 1973).

The treatment of doubly excited states of complex atoms as an effective two-electron hyperspherical problem relies upon the division of the two-electron configuration space into three physically distinct regions (Watanabe, 1982, see Fig. 37). Region I corresponds to the close simultaneous approach of the two outer electrons to the core which is practically forbidden by the centrifugal effects in the energy range of less than 25 eV. Regions II_1 and II_2 correspond to the penetration of one of the outer electrons into the core, independently of the other electron: The problem here reduces to the

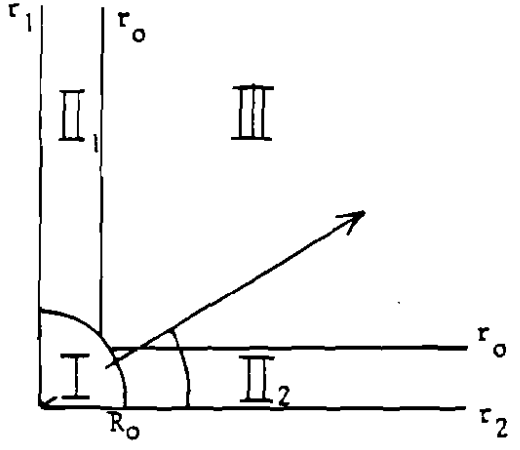

FIG. 37. Division of the (r_1, r_2) plane into three regions. In Region I, both electrons are in the inner region occupied by the core electrons. In Regions II_1 and II_2, one of the electrons enters the core region while the other stays outside. In Region III, the electron pairs stay outside the core; they are under the influence of the attractive potential due to the nucleus and of the core electrons.

scattering of a single electron by the core. In Region III, the core is seen by the electron pair as a mere positive charge. It is in this region where the problem can be reduced to the pure two-electron problems which are to be treated using hyperspherical coordinates.

An efficient method for treating these problems has been initiated by Watanabe (1982). By limiting the solution of the two-electron problems only to Region III, he incorporated the core penetration by one of the electrons by means of a boundary condition at the interfaces between Regions II and III. This is conveniently achieved by adding to the electron-pair Hamiltonian a singular surface operator which enforces the correct boundary condition at the core limits (Bloch, 1957). The Hamiltonian in the restricted Region III reads then:

$$H(1,2) = H_{\text{pair}}(\text{residual}) + \mathcal{L}_{\text{core}}(E) \tag{49}$$

$$\mathcal{L}_{\text{core}}(E) = -\frac{1}{2R^2}[\delta(\alpha - \alpha_0) + \delta(\alpha - \pi/2 + \alpha_0)]\left(\frac{\partial}{\partial\alpha} - L_c(E)\right) \tag{50}$$

where $\alpha_0 = \tan^{-1}(r_0/R)$ and $\pi/2 - \alpha_0$ define the two boundaries between Regions II and III, and $L_c(E)$ defines the logarithmic derivative matrix for the correct emergency of the scattered electron from the core.

Watanabe (1982) used this method to study doubly excited states of He^- near the He($1s2s$, $1s2p$) limits and compared with the results of the experiment of Brunt *et al.* (1977). In their more recent work, Le Dourneuf and Watanabe (1986) extended the method to the doubly excited states of He^- near the He($1sNl$) limits. The two-electron normal modes of the doubly excited states were found not to be broken by the core's perturbation and the states can be classified similarly to the doubly excited states of He and H^-. A more detailed introduction to these voluminous works is not possible here. We only mention that their work provides a good example that doubly excited states of multielectron atoms can be interpreted based upon our understanding of the doubly excited states of two-electron atoms. Detailed discussions of their work can be found in Watanabe *et al.* (1983) and in Le Dourneuf and Watanabe (1986).

There have only been a few preliminary studies of doubly excited states of other atoms. Clark (1984) has examined the CI wave functions of the negative ions of rare gas atoms Ne^-, Ar^-, Kr^-, and Xe^-. By expressing the two-electron part of the wave functions for some of the resonance states in hyperspherical coordinates, it was found that their basic correlation patterns are identical to the corresponding doubly excited states in He and H^-. A more detailed and systematic study of these negative ion resonances is needed to sort out the spectral regularity.

VIII. Concluding Remarks and Perspectives

The study of doubly excited states in this article has centered on the nature and characteristics of correlations of two excited electrons. By representing wave functions in hyperspherical coordinates and examining the symmetry and regularities of the surface charge densities on the (α,θ_{12}) plane, angular and radial correlation are conveniently visualized. The adoption of approximate correlation quantum numbers K, T, and A allows us to systematize correlations and exploit new spectroscopic order of doubly excited states. By analyzing the wave function in the body frame of the atom, these correlation quantum numbers can further be interpreted as being analogous to the moleculelike rovibrational normal modes.

It is recommended that each doubly excited state be designated as ${}_n(K,T)^A_N$ ${}^{2S+1}L^\pi$. This notation contains information about how the two electrons are correlated. This new classification scheme incorporates many important features which are easily revealed by changing one or several quantum numbers:

(1) States with fixed K, T, A, N, L, S, and π but different n belong to the same series. States within the same series have similar correlation patterns. For neutral atoms, the quantum defect along the series is nearly constant. The selection rule for excitation is characteristic of the whole series.

(2) A different "series" can be formed by changing the quantum numbers n and N simultaneously. For example, the series ${}_N(N-1,0)^+_N\,{}^1S^e$ changing with the value of N forms a "double Rydberg series" (Read, 1977; Rau, 1984a). All the states in this series are characterized by having $r_1 = r_2$ and $\theta_{12} = 180°$. For large N, each state behaves like a long linear molecule (Lin, 1982c). The correlations of these states are similar to the Wannier state of two continuum electrons near the double ionization threshold.

(3) States with identical n, N, K, T, and A but different L, S, and π exhibit a rotorlike structure if $A = +1$ or -1 (Section III). Different supermultiplet structure can be obtained by ordering the states according to the number of vibrational nodes in the angle θ_{12} (Section III).

(4) Singly excited states as well as the independent-electron picture are included as a subset of this more general classification scheme.

Most of the works using hyperspherical coordinates have been directed at understanding the structure, particularly resonance states. This success so far has not been extended to scattering problems (Lin, 1975a; Miller and Starace, 1980), nor to excited states where the principal quantum numbers of the two electrons are very different (Park *et al.*, 1985; Fink and Zoller, 1985). The origin of this failure is obvious. Although the hyperspherical coordinates are very close to the independent-particle coordinates in the asymptotic region when one electron is inside and the other is far outside, physically when the two electrons are well separated it is more appropriate to represent the system using the independent-particle coordinates. The small difference between hyperspherical coordinates and independent-particle coordinates at large R introduces a small but ever-present radial coupling between the adiabatic channels. Macek (1985) has shown that it takes the coupling of an infinite number of adiabatic channels at large R to reproduce the independent-particle states in the asymptotic region. Experience (Lin, 1975a) has shown that the elastic scattering phase shifts in e–H scattering at higher energies are not well reproduced by one-channel or a few-channel calculations. This difficulty in obtaining accurate continuum states is responsible for our inability to obtain more accurate decay widths using hyperspherical coordinates.

Attempts to improve the numerical results using the "post-adiabatic" method (Klar and Fano, 1976; Klar, 1977) have not been very successful. Some of the more recent works on the low-lying alkaline earths (O'Mahony, 1985; Watanabe and O'Mahony, 1985; O'Mahony and Greene, 1985) have adopted the R-matrix method to calculate eigenstates and the use of hyperspherical coordinates to analyze the region of configuration space where the coupling occurs. Recognizing the difficulties in applying hyperspherical coordinates to the large-R region, Christensen-Dalsgaard (1984b) proposed a new procedure by matching the inner (small-R) hyperspherical coordinate wave functions onto the outer (large-R) close-coupling wave functions at a hyperradius $R = R_0$. The value of R_0 was chosen where the effects of electron exchange and correlations are small. Preliminary results for the elastic phase shifts in e–H scattering indicate that this procedure eliminates the need of coupling many hyperspherical or many close-coupling channels in each region. Further investigations are needed to test the general usefulness of this procedure.

Extensive analysis of doubly excited states so far has been limited to two-electron atoms only. For doubly excited states with a core structure, the designation presented in this article is adequate for describing the states or channels in the region where correlations are prevalent. In the outer region, the channels are labeled more appropriately in terms of independent-particle quantum numbers. General rules for connecting the two regions have not been established yet. The circumstances where the adiabatic approximation is violated also need to be examined.

Systematic experimental data on doubly excited states are scarce. The approximate selection rules for photoabsorption from the ground state of helium is well established. It is not clear, in view of the lack of experimental data as well as extensive calculations, whether the same selection rules can be applied to photoabsorption from metastable states of helium. There are little

systematics on the cross sections for forming doubly excited states via electron impact or ion impact. Preliminary data from van der Burgt and Heiderman (1985) for e–He collisions seem to indicate that only the + states are excited.

Doubly excited states can be populated using multistep laser excitations in which each of the two valence electrons of alkaline earth atoms are excited separately (Gallagher, 1986). So far, almost all the data pertain to doubly excited states of barium, and the principal quantum numbers of the two electrons are quite different. Because of the lack of calculations, it is not possible to know whether the doubly excited states populated in these experiments belong to the $A = +1$ channels only or whether the $A = -1$ and 0 channels are also populated. Doubly excited states can also be selectively populated via double charge-transfer processes by suitably choosing the projectile–target combinations. Although there are many doubly excited states produced this way, the limited resolutions available so far do not permit the identification of individual states.

The theoretical methods and procedures discussed in this article can be further extended to three-electron systems to study triply excited states. Although there are a few calculations for triply excited states using hyperspherical coordinates (Clark and Greene, 1980; Watanabe *et al.*, 1982; Greene and Clark, 1984), there is very limited information about the correlations of these systems. Preliminary study of excitations beyond triply excited states so far is limited to the properties of hyperspherical harmonics (Cavagnero, 1984, 1985).

ACKNOWLEDGMENTS

I am greatly indebted to Professor U. Fano, who introduced me to the subject of doubly excited states many years ago. I also want to thank many colleagues, whose works are inadequately represented here, who have contributed significantly to the present-day understanding of doubly excited states. The preparation of this article and the underlying research have been supported by the U.S. Department of Energy, Office of Basic Energy Sciences, Division of Chemical Sciences.

REFERENCES

Bloch, C. (1957). *Nucl. Phys.* **4**, 503.
Broad, J., and Reinhardt, W. P. (1976). *Phys. Rev. A* **14**, 2159.
Brunt, J. N. M., King, G. C., and Read, F. H. (1977). *J. Phys. B* **10**, 433.
Bryant, H. C., Dieterle, B. D., Donahue, H., Sharifian, H., Tootoonchi, H., Wolfe, P. A. M., and Yates-Williams, M. A. (1977). *Phys. Rev. Lett.* **38**, 228.

Bryant, H. C., Clark, D. A., Butterfield, K. B., Frost, C. A., Donahue, J. B., Gram, P. A. M., Hamm, M. E., Hamm, R. W., Pratt, J. C., Yates, M. A., and Smith, W. W. (1983). *Phys. Rev. A* **27**, 2889.
Buckman, S. J., Hammond, P., King, G. C., and Read, F. H. (1983). *J. Phys. B* **16**, 4219.
Burke, P. G. (1968). *Adv. At. Mol. Phys.* **4**, 173.
Burke, P. G., and McVicar, D. D. (1965). *Proc. Phys. Soc. (London)* **86**, 989.
Burke, P. G., and Taylor, A. J. (1966). *Proc. Phys. Soc. (London)* **88**, 665.
Callaway, J., and Rau, A. R. P. (1978). *J. Phys. B* **11**, L289.
Cavagnero, M. J. (1984). *Phys. Rev. A* **30**, 1169.
Christensen-Dalsgaard, B. L. (1984a). *Phys. Rev. A* **29**, 470.
Christensen-Dalsgaard, B. L. (1984b). *Phys. Rev. A* **29**, 2242.
Clark, C. W. (1984). *In* "Invited Papers to Electron Correlation Effects and Negative Ions" (T. Anderson *et al.*, eds.) p. 49. Aarhus, Denmark.
Clark, C. W., and Greene, C. H. (1980). *Phys. Rev. A* **21**, 1786.
Cooper, J. W., Fano, U., and Prats, F. (1963). *Phys. Rev. Lett.* **10**, 518.
Crane, M., and Armstrong, L., Jr. (1982). *Phys. Rev. A* **26**, 694.
Ezra, G. S., and Berry, R. S. (1982). *Phys. Rev. A* **25**, 1513.
Ezra, G. S., and Berry, R. S. (1983). *Phys. Rev. A* **28**, 1973, 1989.
Fano, U. (1969). *In* "Atomic Physics" (B. Bederson, V. W. Cohen, and F. M. Pichanick, eds.), Vol. 1, p. 209. Plenum, New York.
Fano, U. (1981). *Phys. Rev. A* **24**, 2402.
Fano, U. (1983). *Rep. Prog. Phys.* **46**, 97.
Fano, U., and Lin, C. D. (1975). *In* "Atomic Physics" (G. zu Putlitz, Weber, and A. Winnacher, eds.), Vol. 4, p. 47. Plenum, New York.
Fink, M., and Zoller, P. (1985). *J. Phys.* **B18**, L373.
Gailitis, M., and Damburg, R. (1963). *Proc. Phys. Soc. London* **82**, 192.
Gallagher, T. F. (1985). *Proc. Int. Conf. Phys. Electron. At. Collisions, 14th, Palo Alto.*
Gram, P. A. M., Pratt, J. C., Yates-Williams, M. A., Bryant, H. C., Donahue, J. B., Sharifian, H., and Tootoonchi, H. (1978). *Phys. Rev. Lett.* **38**, 228.
Greene, C. H. (1981). *Phys. Rev. A* **23**, 661.
Greene, C. H., and Clark, C. W. (1984). *Phys. Rev. A* **30**, 2161.
Herrick, D. R. (1975). *Phys. Rev. A* **12**, 413.
Herrick, D. R. (1983). *Adv. Chem. Phys.* **52**, 1.
Herrick, D. R., and Kellman, M. E. (1980). *Phys. Rev. A* **21**, 418.
Herrick, D. R., and Sinanoglu, (1975a). *Phys. Rev. A* **11**, 97.
Herrick, D. R., and Sinanoglu, (1975b). *J. Chem. Phys.* **62**, 886.
Herrick, D. R., Kellman, M. E., and Poliak, R. D. (1980). *Phys. Rev. A* **22**, 1517.
Ho, Y. K. (1983). *Phys. Rep.* **99**, 1.
Ho, Y. K., and Callaway J. (1983). *Phys. Rev. A* **27**, 1887.
Ho, Y. K., and Callaway J. (1984). *J. Phys. B* **17**, L559.
Iachello, F., and Rau, A. R. P. (1981). *Phys. Rev. Lett.* **47**, 501.
Kellman, M. E., and Herrick, D. R. (1978). *J. Phys. B* **11**, L755.
Kellman, M. E., and Herrick, D. R. (1980). *Phys. Rev. A* **22**, 1536.
Klar, H. (1977). *Phys. Rev. A* **15**, 1452.
Klar, H., and Fano, U. (1976). *Phys. Rev. Lett.* **37**, 1132.
Klar, H., and Klar, M. (1978). *Phys. Rev. A* **17**, 1007.
Klar, H., and Klar, M. (1980). *J. Phys. B* **13**, 1057.
Le Dourneuf, M., and Watanabe, S. (1986). *J. Phys. B.* preprint.
Lin, C. D. (1974a). *Astrophys. J.* **187**, 385.
Lin, C. D. (1974b). *Phys. Rev. A.* **10**, 1986.

Lin, C. D. (1975a). *Phys. Rev. A* **12**, 493.
Lin, C. D. (1975b). *Phys. Rev. Lett.* **35**, 1150.
Lin, C. D. (1976). *Phys. Rev. A* **14**, 30.
Lin, C. D. (1981). *Phys. Rev. A* **23**, 1585.
Lin, C. D. (1982a). *Phys. Rev. A* **25**, 76.
Lin, C. D. (1982b). *Phys. Rev. A* **25**, 1535.
Lin, C. D. (1982c). *Phys. Rev. A* **26**, 2305.
Lin, C. D. (1983a). *Phys. Rev. A* **27**, 22.
Lin, C. D. (1983b). *J. Phys. B* **16**, 723.
Lin, C. D. (1983c). *Phys. Rev. A* **28**, 99.
Lin, C. D. (1983d). *Phys. Rev. Lett.* **51**, 1348.
Lin, C. D. (1984). *Phys. Rev. A* **29**, 1019.
Lin, C. D. (1986). *Proc. Int. Symp. Few Body Methods. Nanning, PRC.*
Lin, C. D., and Macek, J. H. (1984). *Phys. Rev. A* **29**, 2317.
Lipsky, L., Anania, R., and Conneely, M. J. (1977). *At. Data Nucl. Data Tables* **20**, 127.
Macek, J. H. (1968). *J. Phys. B* **1**, 831.
Macek, J. H. (1985). *Phys. Rev. A* **31**, 2162.
Madden, R. P., and Codling, K. (1963). *Phys. Rev. Lett.* **10**, 516.
Madden, R. P., and Codling, K. (1965). *Astrophys. J.* **141**, 364.
Manz, J. (1985). *Comments At. Mol. Phys.* (to be published).
Miller, D., and Starace, A. F. (1980). *J. Phys. B* **13**, L525.
Morse, P. M., and Feshbach, H. (1953). "Methods of Theoretical Physics," p. 1730. McGraw-Hill, New York.
Nikitin, S. I., and Ostrovsky, V. N. (1976). *J. Phys. B* **9**, 3134.
Nikitin, S. I., and Ostrovsky, V. N. (1978). *J. Phys. B* **11**, 1681.
O'Mahony, P. F. (1985). *Phys. Rev. A* (submitted).
O'Mahony, P. F., and Greene, C. H. (1985). *Phys. Rev. A.* **31**, 250.
O'Mahony, P. F., and Watanabe, S. (1985). *J. Phys. B* (submitted).
Park, C. H., Starace, A. F., Tan, J., and Lin, C. D. (1985). *Phys. Rev. A* (submitted).
Percival, I. C., and Seaton, M. J. (1957). *Proc. Cambridge Philos. Soc.* **53**, 654.
Rau, A. R. P. (1984a). *In* "Atomic Physics" (R. S. Van Dyck, Jr. and E. N. Fortson, eds.), Vol. 9. World Scientific, Singapore.
Rau, A. R. P. (1984b). Private communication.
Read, F. H. (1977). *J. Phys. B* **10**, 449.
Rehmus, P. and Berry, R. S. (1979). *Chem. Phys.* **38**, 257.
Rehmus, P. and Berry, R. S. (1981). *Phys. Rev. A* **23**, 416.
Rehmus, P., Kellman, M. E., and Berry, R. S. (1978). *Chem. Phys.* **31**, 239.
Schulz, G. J. (1973). *Rev. Mod. Phys.* **45**, 378.
van der Burgt, P. J. M., and Heideman, H. G. M. (1985). *J. Phys. B* (submitted).
Warner, J. W., Bartell, L. S., and Blinder, S. M. (1980). *Int. J. Quantum Chem.* **18**, 921.
Watanabe, S. (1982). *Phys. Rev. A* **25**, 2074.
Watanabe S., and Greene, C. H. (1980). *Phys. Rev. A* **22**, 158.
Watanabe S., and Lin, C. D. (1986). *Phys. Rev. A* to be published.
Watanabe, S., Le Dourneuf, M., and Pelamourgues, L. (1982). *Colloq. Int.* **334**, *J. Phys. Suppl.* **43**, 223.
Weiss, A. W. (1974). *Phys. Rev. A* **9**, 1524.
Wendoloski, J. J., and Reinhardt, W. P. (1978). *Phys. Rev. A* **17**, 195.
Woodruff, P. R., and Samson, J. A. (1982). *Phys. Rev. A* **25**, 848.
Wulfman, C. E. (1973). *Chem. Phys. Lett.* **23**, 370.